Self-oscillatory instability of the driven phase front propagation induced by liberation of latent heat

Alexei Boulbitch [1,*] and Alexander L. Korzhenevskii [2]
[1]*Zum Waldeskühl 12, 54298 Igel, Germany*
[2]*Institute for Problems of Mechanical Engineering, RAS, Bol'shoi prosp. V. O. 61, 199178 St. Petersburg, Russia*

(Received 9 August 2022; revised 22 March 2023; accepted 26 April 2023; published 13 July 2023)

We theoretically address crystals exhibiting first-order phase transformations subjected to a steadily propagating temperature gradient. The latter drives a nonisothermal propagation of a phase front. We theoretically demonstrate that for the phase transformations of the displacive type, the phase front always steadily follows the isotherm. In contrast, in the case of the order-disorder or hybrid phase transformations in a crystal containing pinning defects, one finds a velocity of the isotherm, the first critical velocity, at which the steady front motion becomes unstable, and a stick-slip front propagation starts. Upon reaching the second critical velocity, the stick-slip behavior vanishes, and the motion becomes steady again. Our results enable one to determine the activation energy of the leading order-disorder process from the measurements of the driven motion of the phase front. In light of these results, we discuss experimental findings for $PbTiO_3$ and $NaNbO_3$

DOI: 10.1103/PhysRevE.108.014114

I. INTRODUCTION

In crystals exhibiting first-order phase transitions, the transformation process involves the motion of phase fronts. The front propagation liberates the transformation heat. Since the phase front velocity depends on temperature, evolving of the heat influences the front dynamics, its action representing feedback, positive or negative. The positive feedback may give rise to the instability of the phase front's steady motion giving rise to a propagation mode during which the front velocity exhibits self-oscillations. One refers to this mode as the *self-oscillating, stick-slip*, or *jerky* motion.

Experiments with the phase front motion require controlling its thermodynamic driving force. A specially designed furnace developed by Burfoot and Parker [1] fulfills this challenging task. The furnace generates a temperature gradient, $J = \nabla\Theta$, along the sample, where Θ is the temperature. One drives the isotherm along the crystal with a velocity V by cooling or heating the sample's butt ends with a prescribed rate (see Sec. II for details). So far, experiments with such a furnace have been performed on two crystals: $PbTiO_3$ [2–8] and $NaNbO_3$ [5,8,9].

In experiments with $PbTiO_3$, the dynamics of the interface between the cubic (Pm3m) and tetragonal (P4mm) phases have been studied. They revealed a velocity interval $V_{*1} < V < V_{*2}$ within which the phase front exhibits the stick-slip motion. It transforms into relaxational oscillations at V close to V_{*2}. At $V < V_{*1}$ and $V > V_{*2}$, the phase front steadily follows the isotherm. Upon increasing the heat sink, the jerky mode vanished [3–7].

In $NaNbO_3$, the phase front between Pnmm and Pbma phases exhibited the self-oscillating motion at $0 < V < V_{*2}$ and the steady one otherwise [5,8,9].

In addition to the dynamics of the crystal-crystal phase transformations, one observes self-oscillations of the front in two other classes of phenomena in solids: (1) explosive crystallization and (2) gasless fuel combustion.

Explosive crystallization represents a fast transformation from the amorphous to the crystalline phase, taking place in some amorphous semiconductors, amorphous metallic alloys, amorphous metals, and dielectrics. In experiments, one often drives the explosive crystallization front by a scanning laser spot. The self-oscillations manifest themselves in a generation of alternating crystalline and amorphous layers, their shape and spatial regularity varying depending on the experimental conditions [10]. Using high-resolution dynamic transmission electron microscopy, Egan and coauthors observed the internal structure of the layers and the dynamics of its formation in amorphous germanium during the laser-driven crystallization [11].

Gasless combustion represents a chemical reaction in the solid phase involving no oxygen or other gases. If the activation energy is high, the reaction localizes within a narrow region, which one regards as a combustion front. The transformation of the steady regime to the self-oscillating one first observed by Merzhanov, Filonenko, and Borovinskaya [12] takes place during the gasless combustion of various fuels [13].

A limited number of theoretical works address the front motion in areas as different as explosive crystallization, gasless combustion, and crystal-crystal phase transformation. These three phenomena exhibit, however, the same instabilities, and one describes them by similar mathematical apparatus.

Shklovskii has studied the amorphous-to-crystal transition [14] as well as Kurtze, van Saarloos, and Weeks [15–18]. This transition requires overcoming an energetic barrier. Thus, the front velocity obeys the Arrhenius law. The latter acts as a mechanism for positive feedback: the velocity dramatically

*aboulbitch@gmx.de

increases with the growing temperature. Kurtze, van Saarloos, and Weeks demonstrated that under certain conditions, both self-sustained and driven by a propagating laser spot, the front motion passes into a self-oscillating regime [15–18]. Makhviladze and Novozhilov have theoretically described self-oscillations of the reaction front during the gasless combustion [19,20].

Gordon studied the first-order transition dynamics during the crystal-crystal phase transformation within the framework of the time-dependent Ginzburg-Landau equation. He demonstrated its exact solution. The latter describes the phase front propagating with a constant velocity in an overcooled or overheated crystal [21]. Gordon and coauthors used this approach to describe the transition kinetics of various types of solids: ferroelectrics, magnetics, improper ferroelectrics, and others [22,23]. Gordon's solution is, however, isothermal; it neglects heat liberation.

Umantsev and Roitburd were the only ones who studied the phase front motion accompanied by the heat liberation during the crystal-crystal phase transformation [24]. Based on the time-dependent Ginzburg-Landau theory with a temperature-independent kinetic factor, they derived the heat transfer equation valid in this case. Below, we start with their result. They further studied the effect of heat liberation on the steady propagation of the phase front and concluded the front self-oscillations to be impossible [24,25].

It is a common opinion that instability of the steady motion during the explosive crystallization qualitatively differs from that during crystal-crystal transition [14–18]. In both cases, the front propagation is followed by a heat release. In the former case, it is the heat of the glass state decay; in the latter, it is the latent heat of the transformation. The velocity of the explosive crystallization front is highly nonlinear in temperature since it obeys the Arrhenius law. Therefore, the transition heat release accelerates the front propagation in the former case. The evolving heat, thus, acts as positive feedback leading to steady motion instability.

In contrast, in the case of the transitions from the high- to low-temperature phase in $PbTiO_3$ and $NaNbO_3$ [2–9] the phase front propagation requires overcooling. The latent heat release decreases the overcooling, thus, slowing the front down. That is, the heat evolving generates negative feedback. These arguments led one to the belief that crystal-melt or crystal-crystal front propagation must always be steady [14–18]. The latter contradicts, however, the experimental observations [2–9].

Thus, since its experimental discovery in 1975 [2], one has to do with an unexplained paradox. It motivated us to study the dynamics of the phase interface in crystals exhibiting structural phase transformations.

This paper theoretically studies a crystal exhibiting the first-order phase transition between two crystalline phases placed into the gradient furnace. We describe the transition within the Ginzburg-Landau approach supplemented with the heat transfer equation. We propose to apply the Arrhenius kinetics to the time-dependent Ginzburg-Landau equation such that it describes both displacive and order-disorder transitions.

Our approach reveals two opposite cases. In the case of the displacive type of phase transformations, the phase front propagation is always steady. The same situation occurs for the order-disorder transition in an ideal (defectless) crystal.

However, the behavior may radically change during order-disorder transformations in a crystal containing pinning defects. We show that, in this case, equations exhibit a bifurcation at a certain velocity of the isotherm $V = V_{*1}$. At V_{*1}, the self-oscillatory motion of the phase front branches off from the steady one. We argue that the stick-slip phase front motion is a fingerprint of the order-disorder or hybrid nature of the phase transformation. We predict that with the further increase of the isotherm velocity, as soon as it achieves a second critical velocity $V = V_{*2}$ ($V_{*2} > V_{*1}$), the stick-slip front motion vanishes, and at $V > V_{*2}$ the front only propagates steadily. We establish a relation between the activation energy ϵ and the second critical velocity V_{*2}. Based on our results, we further discuss the observations of the stick-slip front propagation in $PbTiO_3$ and determine the corresponding activation energy $\epsilon \approx 0.59$ eV. Also, we derive simple analytical relations between the crystal parameters and the front velocity and its critical values. Our results show that measuring the phase front motion can become an additional experimental tool for studying polymorphic phase transitions and extracting their parameters.

The paper is organized as follows. Section II describes the temperature distribution within the oven and introduces the heat transfer equation as well as the time-dependent Ginzburg-Landau one. In Sec. III we move to dimensionless variables and derive the dependence of the velocity on the temperature. In Sec. IV we derive an integro-differential equation describing the phase front motion. We find its solution describing steady front motion. At the end of Sec. IV, we discuss four possible scenarios of the front motion. Section V analyzes the emergence of the self-oscillation motion mode. Section VI discusses the application of our results to the experimental findings obtained on $PbTiO_3$. Finally, Sec. VII provides an overall discussion of our results, and the paper is summarized in Sec. VIII. To support our analysis, some essential steps involved in our calculations are provided in four Appendixes.

II. EQUATIONS OF MOTION AND THERMAL REGIME OF THE PHASE FRONT

A. The temperature distribution within the empty oven

The gradient furnace schematically displayed in Fig. 1(a) maintains distinct values of the temperature, $\Theta_{1,2}$ at two butt ends, 1 and 2 of the sample. These temperatures vary with time T in a controlled fashion. Detailed description of the furnace construction one finds in [1] and [5]. During the measurements, one steadily decreases the temperatures $\Theta_{1,2}$ with the time:

$$\frac{\partial \Theta_{1,2}}{\partial T} = -R, \tag{1}$$

where $R > 0$ is the rate of the temperature decrease. Experiments [2–9] take place during the regime in which the relation (1) holds.

The Péclet number, Pe, for this configuration takes the following form:

$$\mathrm{Pe} = \frac{V d_1}{\chi}, \tag{2}$$

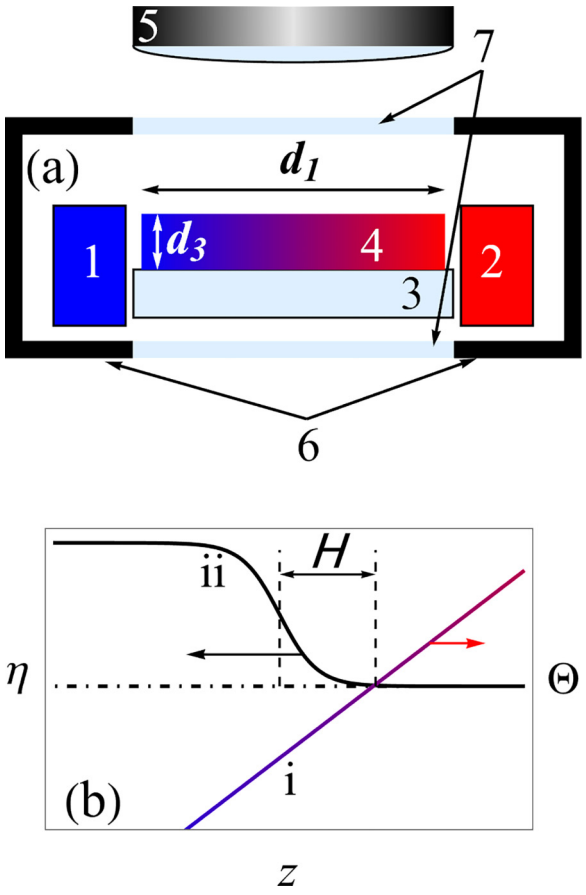

FIG. 1. (a) Schematic view of the oven design. 1 and 2 indicate the heaters with the temperatures Θ_1 and Θ_2 with $\Theta_2 > \Theta_1$. 3 shows the glass substrate, and 4 indicates the crystalline sample. The gradient of the color of its image reflects its temperature gradient. The camera is shown by 5. 6 indicates the housing and 7 the optical windows. (b) Schematic of the temperature distribution $\Theta_{\text{furn}}(z)$ (i, right vertical axis indicated by the right arrow) and the order parameter $\eta(z)$ (ii, left vertical axis, indicated by the left arrow) following the temperature distribution with the lag H. Both propagate from left to right.

where d_1 is the sample length [Fig. 1(a)], V is the isotherm velocity,

$$\chi = \frac{k}{c\rho} \tag{3}$$

is the temperature diffusivity of the crystal, k is its thermal conductivity, ρ is its mass density, and c is the specific heat of the sample. Let us denote a temperature gradient along the furnace as $J = \nabla\Theta$ and a spatial coordinate along the sample, X. If $\text{Pe} \ll 1$, with good accuracy, one can regard the temperature distribution within the furnace as a linear function:

$$\Theta_{\text{furn}}(X, T) = \Theta_{\text{b}} + J(X - VT), \tag{4}$$

and $J = (\Theta_2 - \Theta_1)/d_1$. Let us stress that J describes the part of the temperature gradient only generated by the gradient furnace. It does not account for the heat evolving. We regard J and R as parameters controlled in the experiment.

In this case, one determines the isotherm velocity V by the ratio of the temperature rate and its gradient:

$$V = \frac{R}{J}. \tag{5}$$

In the present paper, we always assume that the inequality $\text{Pe} \ll 1$ holds.

The expression (4) describes the isotherm propagating from left to right with the constant velocity V [the line (i) in Fig. 1(b)]. We selected the form of Eq. (4) such that in the initial moment ($T = 0$), the sample has the binodal temperature Θ_{b} in the point $X = 0$. The propagation of the isotherm forces the phase front to follow it [the line (ii) in Fig. 1(b)]. The optical windows [Fig. 1(a), 7] provide one with the registration of the front motion by the microscope or video camera [Fig. 1(a), 5] and the backlighting.

The temperature $\Theta(X, T)$ in the point X of the crystal in the moment T consists of the furnace temperature Θ_{furn} (4) and its perturbation $\delta\Theta(X, T)$ caused by the heat evolved in the course of the phase transformation. One finds

$$\Theta(X, T) = \Theta_{\text{b}} + J(X - VT) + \delta\Theta(X, T). \tag{6}$$

In the next section, we discuss the equation for the temperature perturbation $\delta\Theta(X, T)$.

B. The time-dependent Ginzburg-Landau equation

One describes the propagation of the phase front along the crystal forced by the temperature gradient by the system of two equations. The first of them is the time-dependent Ginzburg-Landau equation imposed on the order parameter $\eta = \eta(X, T)$ [26]:

$$K\frac{\partial\eta}{\partial T} = G\frac{\partial^2\eta}{\partial X^2} - \alpha_0[\Theta(X, T) - \Theta_{\text{c}}]\eta + \beta\eta^3 - \gamma\eta^5, \tag{7}$$

where $\Theta = \Theta(X, T)$ is the temperature in the point X of the sample, in the time moment T, Θ_{c} is the Curie temperature, and $G > 0$, $\alpha_0 > 0$, $\beta > 0$, and $\gamma > 0$ are the coefficients of the Landau potential. Let us note that we have chosen the sign of β in Eq. (7) such that $\beta > 0$ (7) describes the first-order phase transformation. The classical Landau theory regards the coefficients G, α_0, β, and γ as temperature-independent ones; we also accept this assumption.

Further, $K > 0$ is the kinetic coefficient. Let us recall that one divides all structural phase transformations into two large classes: of the displacive and order-disorder types. The kinetic coefficient K in these classes dramatically differs from one another.

In crystals belonging to the displacive transitions, atoms move in potentials possessing a single minimum. Below the transition point, the minimums of these potentials continuously displace from their original positions in the high-symmetry phase. One can regard the latter process as a condensation of one of the optical phonon modes. For the transitions of the displacive type, $K = K_0 \sim 10^{-13}$s.

In contrast, during the transitions of the order-disorder class, atoms of the elementary cell move within a multiminimum potential and have to overcome an energetic barrier, ϵ. The frequency of their jump attempts has a typical value $\sim K_0$.

Taking this into account, we express the kinetic factor as follows:

$$K = K_0 \exp\left(\frac{\epsilon}{k_B \Theta}\right), \tag{8}$$

where k_B is the Boltzmann's constant. In this form, Eqs. (7) and (8) describe both the order-disorder phase transformations ($\epsilon > 0$) as well as those of the purely displacive class ($\epsilon = 0$).

The first-order phase transformation between two crystalline phases exhibits hysteresis. Within the hysteresis, two phases $\eta = 0$ and $\eta \neq 0$ coexist. One of them, say, $\eta \neq 0$ is stable, while the phase $\eta = 0$ is metastable. The lower spinodal bounds the hysteresis from below at the temperature Θ_{low}. The upper one limits it from above at $\Theta = \Theta_{up}$. The binodal lies between the spinodals: $\Theta_{low} < \Theta_b < \Theta_{up}$.

In this paper, we are interested only in the lower hysteresis part $\Delta\Theta_h$ between the binodal and the lower spinodal: $\Delta\Theta_h = \Theta_b - \Theta_{low}$. Various phase transitions typically exhibit the hysteresis from a few to a few tens of degrees, though, in some solids (such as, e.g., martensites), $\Delta\Theta_h$ achieves several hundred of degrees [27].

It is generally believed that the spinodal cannot be achieved in statics. During the isotherm motion, however, one can achieve a spinodal locally. In such a case, spinodal decomposition will occur under the temperature gradient near the phase front. The thin phase front then turns into a relatively wide layer containing multiple nuclei of the phase $\eta \neq 0$ surrounded by the phase $\eta = 0$.

On the one hand, achieving the spinodal in dynamics can represent a significant scientific interest. On the other hand, however, for the studies performed in [2–9] formation of such a regime means a failed experiment. Indeed, in this case, the abrupt phase boundary does not exist anymore and cannot be followed. The heterophase layer that emerges in its place exhibits strong fluctuations, excluding registration of its position. For this reason, one selects experimental parameters in such a way as to exclude this possibility. From the theoretical point of view, if

$$J d_1 \ll \Delta\Theta_h, \tag{9}$$

the spinodal cannot be reached within the sample. Aiming to address the experiments [2–9] in this paper, we assume that the inequality (9) holds.

C. The thermal conductivity equation

The temperature $\delta\Theta(X, T)$ is subjected to the thermal equation. If the Biot number

$$\mathrm{Bi} = \frac{\Gamma d_3^2}{\chi} \tag{10}$$

is small, it is correct to regard the sample as a thin rod. One characterizes the latter by its longitudinal temperature diffusivity χ. The second parameter characterizing the model is the inverse time, Γ, of the heat exchange between the sample and the environment (including the surrounding air and substrate):

$$\Gamma = \frac{2k_s}{d_3 c \rho}, \tag{11}$$

where k_s is the heat transfer coefficient between the sample and the surrounding, d_3 is the sample height [Fig. 1(a)], and d_2 is its width [not shown in Fig. 1(a)], and we assume that $d_3 \ll d_1, d_2$ [28].

In general, the values of parameters χ_{high} and Γ_{high} in the high-temperature phase differ somewhat from χ_{low} and Γ_{low} in the low-temperature one. We neglect, however, their difference and assume $\chi_{high} = \chi_{low} \equiv \chi$ and $\Gamma_{high} = \Gamma_{low} \equiv \Gamma$.

Assuming that both (2) and (10) hold one finds that the relation (6) and the thin rod approximation are valid. The heat transfer equation takes the following form:

$$\frac{\partial \delta\Theta}{\partial T} = \chi \frac{\partial^2 \delta\Theta}{\partial X^2} - \Gamma \delta\Theta + \frac{\Lambda V}{c} \delta[X - X_f(t)]. \tag{12}$$

Here Λ is the heat evolving due to the phase transition in the point at the current phase front position $X = X_f$, and $\delta(z)$ is the δ function. Making use of Landau theory of phase transitions [26] one finds

$$\Lambda = \frac{3\alpha_0 \beta}{8\gamma} \Theta_b. \tag{13}$$

Equations (7) and (12) provide the complete description of the forced propagation of the phase boundary.

III. DIMENSIONLESS EQUATIONS OF THE FORCED DYNAMICS OF THE PHASE FRONT

A. Rescaling

Let us introduce several dimensionless variables and parameters. Below we use the dimensionless coordinate x and time t defined as follows:

$$x = X \times \left(\frac{\Gamma}{\chi}\right)^{1/2}, \quad t = \Gamma T. \tag{14}$$

Further, we use the dimensionless dependent variables, such as temperature $\theta(x, t)$, its perturbation caused by the heat evolving $\delta\theta(x, t)$, the phase boundary position $x_f(t)$, and the spatial lag $h(t)$ between the isotherm and the phase front. They correspond to the original temperature Θ, its perturbation $\delta\Theta$, the phase front position X_f, and lag H:

$$\theta(x, t) = \frac{\Theta(X, T)}{\Theta_b}, \quad \delta\theta(x, t) = \frac{\delta\Theta(X, T)}{\Theta_b},$$

$$x_f(t) = X_f(T)\left(\frac{\Gamma}{\chi}\right)^{1/2}, \quad h(t) = H(T)\left(\frac{\Gamma}{\chi}\right)^{1/2}. \tag{15}$$

One further introduces 11 dimensionless parameters

$$v = \frac{V}{\sqrt{\chi\Gamma}}, \quad j = \frac{J}{\Theta_b}\sqrt{\frac{\chi}{\Gamma}}, \quad r = \frac{R}{\Gamma\Theta_b},$$

$$\lambda = \frac{\Lambda}{c\Theta_b}, \quad \theta_c = \frac{\Theta_c}{\Theta_b}, \tag{16}$$

$$\phi = \frac{\epsilon}{k_B\Theta_b}, \quad \omega = \frac{\Omega}{\Gamma}, \quad \kappa = K\Gamma, \quad \kappa_0 = K_0\Gamma,$$

$$g = \frac{G\Gamma}{\chi}, \quad n = 0.3\frac{\beta K_0}{\alpha_0 \Theta_b}\left(\frac{\chi\Gamma}{G\gamma}\right)^{1/2}. \tag{17}$$

In the following, the capital letters stay for the original values, and the small letters for the rescaled, dimensionless

ones. In particular, x, v, j, r, λ, ϕ, ω, κ, and g are the rescaled dimensionless coordinate along the crystal, velocity, temperature gradient, temperature rate, parameter characterizing the temperature rise at the phase boundary, energetic barrier normalized by $k_B\Theta_b$, frequency, and coefficients of the rescaled Ginzburg-Landau equation, respectively.

The exceptions are the order parameter η and the coefficients of the Landau potential α_0, β, and γ. We did not rescale these parameters and used the small letters to denote their original values throughout the paper.

Finally, the dimensionless parameter n plays an essential role in our equations below. Let us point out that n is a composition of three dimensionless parameters: $\alpha_0\Theta_b$, $K_0\sqrt{\chi\Gamma/G}$, and $\beta/\sqrt{\gamma}$. However, in the present theory, one meets them only as the combination entering n.

Let us note that the extraordinary complexity of this problem is related to the fact that it depends on 11 dimensionless parameters [(16) and (17)], let alone Pe and Bi.

The rescaled equation for the order parameter one obtains straightforwardly by substitution the replacements (14), (16), and (17) into Eq. (7).

One finally comes to the rescaled equations in the following form:

$$\kappa\frac{\partial\eta}{\partial t} = g\frac{\partial^2\eta}{\partial x^2} - \alpha_0\Theta_b[1 + j(x - vt) + \delta\theta(x,t) - \theta_c]\eta + \beta\eta^3 - \gamma\eta^5, \tag{18}$$

where η is now regarded as $\eta(x,t)$. This equation operates with the rescaled time t and coordinate x, but we did not rescale the order parameter η. The factor $\alpha_0\Theta_b[1 + j(x - vt) + \delta\theta(x,t) - \theta_c]$ in front of η in (18) comes from the factor $\alpha_0[\Theta(X,T) - \Theta_c]$ of Eq. (7). It originates from the temperature-dependent coefficient $\alpha = \alpha_0(\Theta - \Theta_c)$ of the Landau potential. Further, j is the rescaled temperature gradient, and $j(x - vt)$ describes the temperature distribution propagating along the sample. $\delta\theta(x,t)$ is the increase of the rescaled temperature due to the liberated transformation heat, and θ_c is the rescaled Curie temperature. Generally, the physical sense of the terms of Eq. (18) is the same as that of the corresponding terms of (7).

Details on the further derivation of the rescaled thermal equation imposed on the rescaled temperature $\delta\theta = \delta\theta(x,t)$ are found in Appendix A. The rescaled equation reads

$$\frac{\partial\delta\theta}{\partial t} = \frac{\partial^2\delta\theta}{\partial x^2} - \delta\theta + \lambda\dot{x}_f(t)\delta[x - x_f(t)], \tag{19}$$

where $\dot{x}_f(t) \equiv dx_f(t)/dt$.

B. Equation of motion of the phase front

The order parameter $\eta(x,t) = \eta[x - x_f(t)]$ obeys the dynamic equation (18).

The first step of our derivation is to formulate the equation imposed on the phase front's coordinate $x_f(t)$. To derive an approximate, though accurate, equation on $x_f(t)$, let us use the approach of Gordon [21]. Within this approach, one expresses the phase front velocity, $\dot{x}_f$, as follows:

$$\dot{x}_f = \frac{\beta}{\kappa}\sqrt{\frac{g}{\gamma}}\frac{1 + \sqrt{1 - 4\zeta} - 8\zeta}{\sqrt{6(1 + \sqrt{1 - 4\zeta} - 2\zeta)}} \approx 3.32\frac{\beta}{\kappa}\sqrt{\frac{g}{\gamma}}\left(\frac{3}{16} - \zeta\right), \tag{20}$$

where we introduced the following dimensionless parameter ζ:

$$\zeta = \frac{\alpha_0\gamma}{\beta^2}(\Theta - \Theta_c). \tag{21}$$

Let us mention that for the Ginzburg-Landau equation (7), the hysteresis is at $0 \leqslant \zeta \leqslant 1/4$, and the binodal position is $\zeta = 3/16$. More details on the phase diagram can be found e.g., in [26]. The solution (20) is valid at $0 \leqslant \zeta \leqslant 3/16$ between the lower spinodal ($\zeta = 0$) and the binodal ($\zeta = 3/16$). Let us note that the difference between the exact and approximate expressions is at most 14%, and both expressions turn into zero at the binodal at $\zeta = 3/16$, as it should be. One finds

$$\dot{x}_f = \varsigma(\Theta_b - \Theta), \quad \varsigma \approx \frac{3.32\alpha_0\sqrt{g\gamma}}{\beta\kappa}, \tag{22}$$

where one can regard $\varsigma(\Theta_b - \Theta)$ as a driving force for the phase front.

Taking (8), (15), and (17) into account one finds the front velocity $\dot{x}_f(t)$ in the following form:

$$\dot{x}_f(\theta) = \frac{1}{n}(1 - \theta)\exp\left(-\frac{\phi}{\theta}\right). \tag{23}$$

Let us orient the x axis along the normal to the phase front plane coinciding with the temperature gradient's direction. Let us further regard the temperature at the phase boundary as $\theta_f = \theta_f(x_f, t)$:

$$\theta_f(x_f, t) = 1 + j[x_f(t) - vt] + \delta\theta. \tag{24}$$

Substituting this into (23), one finds the equation of the front motion in the following form:

$$\dot{x}_f(t) = -\frac{1}{n}\{j[x_f(t) - vt] + \delta\theta\} \times \exp\left\{-\frac{\phi}{1 + j[x_f(t) - vt] + \delta\theta}\right\}. \tag{25}$$

Together (25) and (19) describe the nonisothermal propagation of the phase front.

We will analyze this system of equations in the following sections.

IV. NONISOTHERMAL PROPAGATION OF THE PHASE FRONT

A. Integro-differential equation of motion of the phase front

Solving (19), we obtain the temperature perturbation $\delta\theta(x_f(t), t) \equiv \delta\theta(t)$ in terms of the phase front velocity $\dot{x}_f(t)$ as follows:

$$\delta\theta(t) = \lambda\int_0^\infty dt'\int_{-\infty}^{\infty}\frac{dq}{2\pi}\dot{x}_f(t - t') \times \exp\{-(q^2 + 1)t' + iq[x_f(t) - x_f(t - t')]\}, \tag{26}$$

where i is the imaginary unit. The derivation of this expression the reader finds in Appendix B.

Substitution of (26) into Eq. (25) yields the equation of motion of the phase front:

$$\dot{x}_{\rm f}(t) = -\frac{\mathfrak{A}(x,t)}{n}[j[x_{\rm f}(t) - vt] + \mathfrak{J}(x,t)], \tag{27}$$

where $\mathfrak{J}(x,t)$ and $\mathfrak{A}(x,t)$ are expressed as follows:

$$\mathfrak{J}(x,t) = \lambda \int_0^\infty dt' \int_{-\infty}^{\infty} \frac{dq}{2\pi} \dot{x}_{\rm f}(t-t') \times \exp\{-(q^2+1)t' + iq[x_{\rm f}(t) - x_{\rm f}(t-t')]\}, \tag{28}$$

$$\mathfrak{A}(x,t) = \exp\left\{-\frac{\phi}{1 + j[x_{\rm f}(t) - vt] + \mathfrak{J}(x,t)}\right\}. \tag{29}$$

Equations (27)–(29) represent a highly nonlinear integro-differential equation with retardation.

B. The steady motion of the phase front

Let us first assume that the isotherm propagates with the dimensionless velocity $v > 0$, while the phase front steadily follows it with the dimensionless lag $h_0 > 0$:

$$x_{\rm f}(t) = vt - h_0. \tag{30}$$

In this case, integrals in (26) are solved exactly yielding

$$\delta\theta = \delta\theta_0 = \frac{v\lambda}{\sqrt{v^2+4}}. \tag{31}$$

Let us define the reduced temperature $\theta_{\rm s}$ on the steadily propagating front as $\theta_{\rm f}$ (24) with $x_{\rm f}$ obeying Eq. (30):

$$\theta_{\rm s} = 1 - jh_0 + \delta\theta_0. \tag{32}$$

Using (23) one obtains the equation

$$v = \frac{1}{n}(1-\theta_{\rm s})\exp\left(-\frac{\phi}{\theta_{\rm s}}\right). \tag{33}$$

One can regard it as the dependence of $\theta_{\rm s}$ on v and ϕ in the parametric form. Its visualization is displayed in Fig. 2(a). One observes that $\theta_{\rm s}$ is a double-valued function of v and ϕ. Its smaller value corresponds to the front running at a larger distance, while the higher value is at a smaller distance from the isotherm.

Regarding the cross section of this surface at a fixed ϕ, one obtains the curve $v = v(\theta_{\rm s})$ shown by the solid line in Fig. 2(b) with the maximum in the point

$$\theta_{\max} = \frac{1}{2}(\sqrt{\phi^2+4\phi} - \phi),$$
$$v_{\max} = \frac{1}{n}\exp\left(-\frac{\phi}{\theta_{\max}}\right)(1-\theta_{\max}). \tag{34}$$

One, further, needs an analytical expression $\theta_{\rm s} = \theta_{\rm s}(v)$ but cannot solve Eq. (33) exactly. In the following we are interested only in the ascending branch of the curve (33) shown in Fig. 2(b). One observes that the expression

$$v \approx v_{\max}\exp[-p(\phi)(\theta_{\rm s} - \theta_{\max})^2] \tag{35}$$

accurately approximates the ascending behavior of $v = v(\theta_{\rm s})$ [as is shown by the dashed line in Fig. 2(b)], provided the function $p(\phi)$ reads as follows:

$$p(\phi) \approx 5.8\phi - 7.2.$$

The latter we obtained by the least square fitting within the physically reasonable interval of the energy barriers 0.3 eV $< \epsilon <$ 0.8 eV. According to (17) with $\Theta_{\rm b} = 766$K (see Table I below) it yields the interval $5 \leqslant \phi \leqslant 12$.

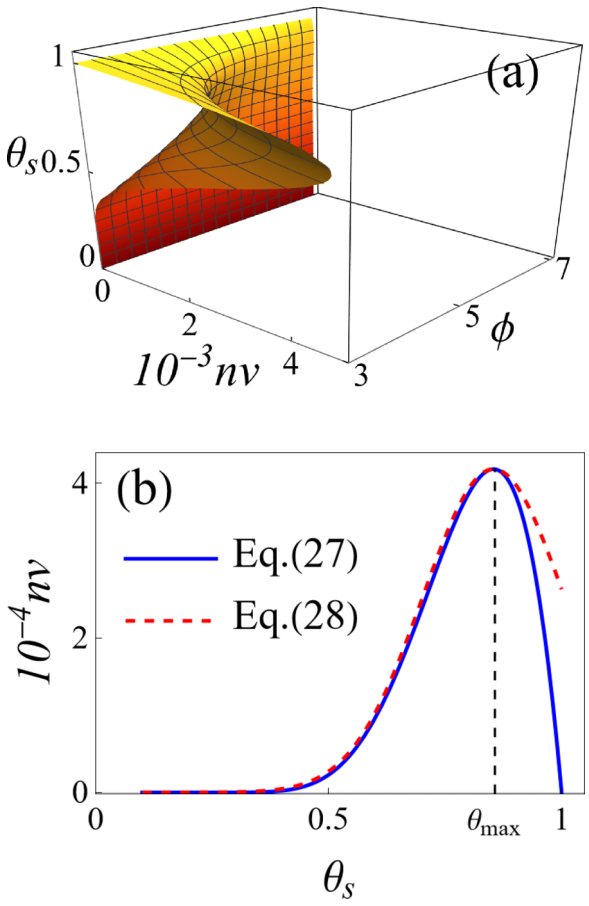

FIG. 2. Dependence of the temperature at the phase front $\theta_{\rm s}$ on v and ϕ. (a) A 3D image showing $\theta_{\rm s} = \theta_{\rm s}(v,\phi)$. (b) The solid line displays the cross section of the surface (33) shown in (a) by the plane $\phi = 10$ showing $v = v(\theta_{\rm s})$. The dashed line demonstrated the run of the expression (35) accurately approximating the expression (33) at the ascending branch.

Using (35), one finds the explicit expression $\theta_{\rm s}(v,\phi)$ at the ascending branch:

$$\theta_{\rm s}(v,\phi) \approx \theta_{\max} - \left[\frac{1}{p(\phi)}\ln\left(\frac{v_{\max}}{v}\right)\right]^{1/2}. \tag{36}$$

Using (32) one finds the lag h_0 during the steady propagation at the ascending branch:

$$h_0 = \frac{1}{j}\left[1 - \theta_{\rm s}(v,\phi) + \frac{v\lambda}{\sqrt{v^2+4}}\right], \tag{37}$$

where $\theta_{\rm s}(\phi)$ is defined by (36).

C. Scenarios of the transformation dynamics

Figure 2(b) displays the $v = v(\theta_{\rm s})$ dependence comprising the ascending branch (to the left from the point of maximum)

TABLE I. Experimental data for $PbTiO_3$.

α_0 (K^{-1})	β ($\frac{cm^3}{erg}$)	γ ($\frac{cm^6}{erg^2}$)	Θ_b (K)	Θ_{low} (K)
3.67×10^{-4} [4,29]	3.58×10^{-13} [29]	2.14×10^{-23} [29]	766 [4,29]	741 [4]
G (cm^2)	K_0 (s)	d_1 (mm)	d_2 (mm)	d_3 (mm)
1.6×10^{-16} [7]	1.0×10^{-13}	2 [3,6,7]	1 [6,7]	0.2 [6,7] 0.03 [3]
μ (g/mol)	ρ (g/cm^3)	Λ (erg/g)	λ	c ($\frac{erg}{gK}$)
3.03×10^2	7.52 [30]	2.14×10^8 [31]	0.067[b]	4.2×10^6 [33]
k ($\frac{erg}{cmgs}$)	χ (cm^2/s)	V_{*1} (μm/s)	V_{*2} (μm/s)	$V_{max}^{(exp)}$ (μm/s)
4×10^5 [32]	0.019[a]	110 [5]	500 [5]	500[c]

[a]Calculated according to (3).
[b]Calculated according to the expression from (16).
[c]Obtained by us by fitting of the experimental data taken from [6] as shown in Fig. 8.

and the descending one. Qualitatively, it has a form closely resembling the one that has been first analyzed by Shklovskii [14]. For the explosive crystallization, Kurtze, van Saarloos and Weeks demonstrated that the ascending branch gives rise to the stick-slip phase front propagation [15–18].

The kinetics of the first-order phase transformation between crystalline phases essentially differs from the explosive crystallization due to its interplay with hysteresis. The phase front discussed here can exist only if the sample is in the lower hysteresis part $\Theta_{low} \leqslant \Theta \leqslant \Theta_b$. The combination of the latter inequality with the specific dependence of the velocity on temperature shown in Fig. 2(b) defines the variety of the scenarios of the front propagation. We qualitatively address these scenarios below in the present section.

We derived the relation between the rescaled phase front velocity $\dot{x}_f$ and rescaled temperature θ (23). For the discussion that follows, we write it in original variables:

$$\dot{X}_f(\Theta) = \frac{\alpha_0 \Theta_b \sqrt{G\gamma}}{\beta K_0} \left(1 - \frac{\Theta}{\Theta_b}\right) \exp\left(-\frac{\epsilon}{k_B \Theta}\right). \qquad (38)$$

1. The displacive transitions

In the case of the displacive transition ($\epsilon = 0$) the function $\dot{X} = \dot{X}(\Theta)$ (38) becomes linear [Fig. 3(a)]. In this case, $\dot{X}_f(\Theta)$ represents an interval of the straight line [Fig. 3(a) ii]. It turns into zero at $\Theta = \Theta_b$ [Fig. 3(a) i] and ends up at $\Theta = \Theta_{low}$ [Fig. 3(a) iii].

As the first step of the analysis, let us assume that the sample is subjected to the motionless temperature gradient $R = 0$ yielding $V = 0$. In this case, the phase front temperature coincides with the isotherm $\Theta = \Theta_b$, and its velocity is $\dot{X} = 0$. This state is shown by the arrow (i) in Fig. 3(a).

Next, let us assume that the isotherm moves forward with the velocity V, and the front falls back, allowing the isotherm to run forward over the lag H_0. The lag "translates" into overcooling. At a certain lag, the phase front becomes overcooled enough to propagate, keeping pace with the isotherm. This state of motion is shown by (ii) in Fig. 3(a).

If one increases the isotherm velocity V further, the point showing the state of motion displaces to the left, upwards along the line (ii) in Fig. 3(a).

2. The order-disorder transitions ($\epsilon > 0$)

In this case, the curve $\dot{X} = \dot{X}(\Theta)$ (38) exhibits maximum at $\Theta = \Theta_{max} < \Theta_b$ as is shown in Figs. 3(b)–3(d). The two cases are possible in this situation: Fig. 3(b) $\Theta_{max} < \Theta_{low}$ and Figs. 3(c) and 3(d) $\Theta_{max} > \Theta_{low}$.

The case (b) $\Theta_{max} < \Theta_{low}$. If $\Theta_{max} < \Theta_{low}$ and $\epsilon > 0$, the front velocity $\dot{X}(\Theta)$ exhibits ascending and descending

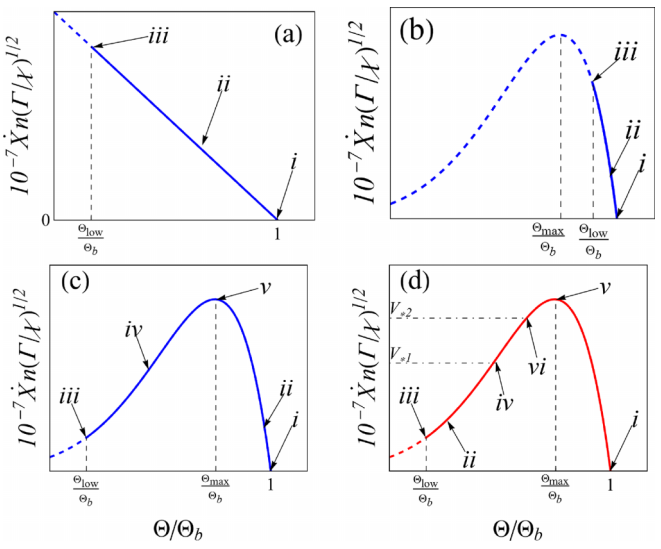

FIG. 3. Illustration for possible scenarios of the phase front propagation. (a) The case of the displacive transitions ($\epsilon = 0$). Panels (b), (c), and (d) correspond to the order-disorder transitions ($\epsilon > 0$) and demonstrate possible ways of the hysteresis interplay with the velocity dependence on temperature $\dot{X}(\Theta)$. Panel (b) illustrates the phase front propagation if $\Theta_{low} > \Theta_{max}$. Panels (c) and (d) display the opposite case: $\Theta_{low} < \Theta_{max}$. Panel (c) attributes to the phase front motion in a defect-free crystal. Panel (d) relates to the phase front initially pinned down by surface defects. In all the panels, (i) shows the point of the binodal. At this point the front is at rest $V = 0$. (ii) indicates the state of the motion with $V > 0$. (iii) shows the point Θ_{low}. (iv) points out the ascending branch, (v) marks the point of maximum of the curve, and (vi) shows the place where the front achieves the second critical velocity V_{*2}. The scenarios are described in the text.

branches separated by the point of maximum at $\Theta = \Theta_{\max}$. Figure 3(b) shows this situation. The lower spinodal point finds itself at the descending branch indicated by the arrow (iii).

At the zero isotherm velocity $V = 0$ one finds $\Theta = \Theta_b$ and $\dot{X} = 0$ [arrow (i) in Fig. 3(b)]. Increasing the isotherm velocity forces the front to fall back over the lag H_0 behind the isotherm. The latter gives rise to the local overcooling until the front's velocity equals the isotherm velocity V [arrow (ii) in Fig. 3(b)]. One concludes that the motion takes place only at the descending branch. Here any increase in the front velocity gives rise to an increase in its temperature. The latter decreases its velocity. If the front velocity decreases, its temperature decreases, increasing its velocity. Thus, the negative feedback takes place at the descending branch. Therefore, the motion at this branch exhibits no instability.

With the further increase of the isotherm velocity V, the front finds itself close to the spinodal point [arrow iii in Fig. 3(b)] with the effect of the spinodal decomposition like the one mentioned previously (Sec. II B].

The case (c) $\Theta_{\max} > \Theta_{\text{low}}$*, an ideal crystal.* If $\Theta_{\max} > \Theta_{\text{low}}$ and $\epsilon > 0$ the $\dot{X}(\Theta)$ dependence exhibits a maximum [Fig. 3(c)] and the lower spinodal hits the curve at the ascending branch [arrow iii in Fig. 3(c)].

As in the previous cases, at $V = 0$, one finds $\Theta = \Theta_b$, and the front is at rest ($\dot{X} = 0$), the isotherm staying at the left butt end of the crystal. The arrow i in Fig. 3(c) indicates this state. As soon as the isotherm starts slowly moving ($V > 0$), the phase front easily slips off from the butt end, staying at the distance H_0 behind the isotherm. The slowly moving isotherm is shown by ii at the descending branch in Fig. 3(c).

The form of the curve shown in Fig. 3(c) does not suggest that the phase front can move with the velocity $V > V_{\max}$ corresponding to the maximum point [v at Fig. 3(c)] of $\dot{X}(\Theta)$ curve. Indeed, despite the physical possibility of driving the isotherm with any velocity, no temperature value corresponds to $V > V_{\max}$. The latter contradiction resolves as follows. The form $\dot{X}(\Theta)$ shown in Figs. 3(b)–3(d) we obtained within the framework of Gordon's solution. One derived the latter using the automodel assumption: $\eta(X, T) = \eta(X - VT)$ [21], describing the translation of the order parameter distribution as a whole from left to right with the velocity V. The absence of the states of motion with $V > V_{\max}$ means that at $V > V_{\max}$, the automodel solution fails. The front, nevertheless, also exists at $V > V_{\max}$. However, in addition to its translation from left to right, a simultaneous relaxation occurs here: $\eta(X, T) = \eta(X - VT, T)$. One concludes that a new type of bifurcation must occur somewhere at $V \leqslant V_{\max}$ where the automodel type of behavior transforms into a nonautomodel one. Looking ahead, let us point out that the bifurcation from the self-oscillating motion to the steady one takes place shortly before the velocity achieves the value $V = V_{\max}$, as one can see from Fig. 5 (ii) and (iii). The complete solution of the problem accounting both for the automodel and nonautomodel behaviors should show a continuous curve also at $\dot{X} > V_{\max}$, the velocity increasing with decreasing the temperature. We do not consider here the nonautomodel regime.

One concludes that in the ideal crystal, the motion's state always appears at the descending branch, the feedback is always negative, and self-oscillations never occur.

The case (d) $\Theta_{\max} > \Theta_{\text{low}}$*, a nonideal crystal.* Let us now consider a crystal with $\epsilon > 0$ and $\Theta_{\max} > \Theta_{\text{low}}$ containing pinning defects at the left butt end surface of the crystal able to arrest the phase front. To break loose from the pinned state, the thermodynamical driving force, $\sim\Theta_b - \Theta > 0$, must reach a critical value. The latter "translates" into a considerable value of the lag H_0, arranging the possibility that the state of the front motion corresponds to the ascending branch of the curve [arrow iv Fig. 3(d)]. At small velocities [arrow ii in Fig. 3(d)], the phase front propagates steadily analogously to those we described in cases (a)–(c) with a somewhat more significant lag H_0. The self-oscillations start as soon as V achieves the first critical velocity V_{*1} [point iv in Fig. 3(d)]. With the increase of the isotherm velocity, the self-oscillations gradually assume a relaxational character. The latter exhibits a period comprising a time interval during which the motion is slow. The fast motion interval follows the slow one [34]. During the former interval, the phase front falls back behind the isotherm. It rapidly accelerates to catch up with it during the latter one. Upon achieving the second critical velocity V_{*2} [point vi in Fig. 3(d)], the stick-slip motion vanishes.

Let us stress the difference between cases (c) and (d). In case (c) of the defect-free crystal, at the beginning of the motion (small V), the front finds itself at the descending branch [ii in Fig. 3(c)]. In contrast, in crystals with surface defects (case d), they pin the front down, forcing it to the ascending branch [ii in Fig. 3(d)]. Thus, pinning plays a crucial role. Let us also mention that distributed weak bulk pinning defects have the same effect on the front motion as discussed in Sec. VII B 3.

Below, we focus on case (d) and study the formation of the self-oscillating motion at the ascending branch.

V. THE OSCILLATORY INSTABILITY OF THE STEADY MOTION

A. Condition of instability

In the following, let us look for the solution $x_f(t)$ in the following form:

$$x_f(t) = vt - h_0 + h_1(t), \tag{39}$$

where we will assume the dimensionless variable $h_1(t)$ to be small: $h_1(t) \ll 1$, while h_0 satisfies (37). Let us rewrite the integro-differential equation (27) in terms of $h_1(t)$. It takes the following form:

$$\widehat{L}h_1 = N(h_1). \tag{40}$$

Here $N(h_1)$ comprises all terms nonlinear in $h_1(t)$ and its derivatives, and $N(0) = 0$. We do not use it in this paper; therefore, we do not write its cumbersome explicit form here.

$\widehat{L}$ is the linear integro-differential operator acting on $h_1(t)$ defined as follows:

$$\widehat{L}h_1 = \mu v^{-1}\dot{h}_1(t) - jh_1(t) - \frac{\lambda}{2\pi}\int_0^\infty dt' \int_{-\infty}^{\infty} dq \times \Phi(h_1, \dot{h}_1, t, t', q)\exp[-(q^2 + 1 - iqv)t'], \tag{41}$$

where

$$\Phi(h_1, \dot{h}_1, t, t', q) = iqv[h_1(t) - h_1(t - t')] + \dot{h}_1(t - t').$$

Furthermore, we introduced a dimensionless parameter μ:

$$\mu = \frac{\theta_s \exp\left(\frac{\phi}{\theta_s}\right)}{\phi - \phi\theta_s - \theta_s^2}. \tag{42}$$

One can see that μ is positive at $\theta_s < \theta_{max}$ and negative otherwise. Using the approximate solution (36), one finds

$$\mu \approx \frac{1}{2\sqrt{p(\phi)\ln(v_{max}/v)}}. \tag{43}$$

Equation (40) has the trivial solution $h_1(t) \equiv 0$.

As soon as the parameters j, λ, and v take such values that the equation

$$\widehat{L}\psi = 0 \tag{44}$$

has a nontrivial solution ψ, Eq. (40) exhibits a bifurcation [35]. The eigenfunction ψ of Eq. (44) has the following form:

$$\psi(t) = \exp(i\omega t), \tag{45}$$

where ω is the dimensionless frequency introduced in (17). Substitution of (45) into (44) yields the relation imposed on the parameters v, μ, j, and λ, which one should regard as the equation to determine the eigenvalue of Eq. (44):

$$\Sigma(\omega, j, \lambda, v) = \frac{2j}{\lambda} - 2i\frac{\mu\omega}{\lambda v} + \frac{v^2 + 2i\omega}{\sqrt{v^2 + 4i\omega + 4}} - \frac{v^2}{\sqrt{v^2+4}} = 0. \tag{46}$$

As soon as the equality (46) holds at some frequency value ω_0, the nonlinear integro-differential equation (40) exhibits a bifurcation. At this point, the trivial solution $h_1 = 0$ becomes unstable, and the periodic solution $h_1(t) \sim \exp(i\omega_0 t)$ branches off from the trivial one [35].

The existence of the solution of (46), however, imposes a relation on the parameters j, λ, ϕ, and v. In the parametric space, this relation specifies a bifurcation hypersurface. Below we address the analysis of the bifurcation condition (46).

B. Analysis of the instability conditions

1. The spectral equations

One observes that (46) is a complex equation, and, therefore, it is equivalent to a system of two real ones: $f_1 = \mathrm{Re}[\Sigma(\omega, j, \lambda, v)]$ and $f_2 = \mathrm{Im}[\Sigma(\omega, j, \lambda, v)]$. Expanding (46) in series at $|\omega| \ll 1$, one finds the following equations:

$$f_1(\omega) \approx \frac{j}{\lambda} - \frac{(v^2-8)}{(v^2+4)^{5/2}}\omega^2 + \frac{5(3v^2-16)}{(v^2+4)^{9/2}}\omega^4 = 0$$
$$f_2(\omega) \approx \left(\frac{4}{(v^2+4)^{3/2}} - \frac{\mu}{\lambda v}\right)\omega + \frac{4(v^2-6)}{(v^2+4)^{7/2}}\omega^3 = 0. \tag{47}$$

By direct comparison of the curves shown in Fig. 4 with plots of $\mathrm{Re}[\Sigma(\omega)]$ and $\mathrm{Im}[\Sigma(\omega)]$ (not shown) at various ranges of ω, one finds that up to $\omega \lesssim 10$ the curves $\mathrm{Re}(\Sigma)$ and $\mathrm{Im}(\Sigma)$ have qualitatively the same form. Quantitatively they are reasonably close to those for $f_1(\omega)$ and $f_2(\omega)$. This fails above $\omega = 10$. Thus, up to $\omega \sim 10$ Eqs. (47) still give a reasonable approximation of (46).

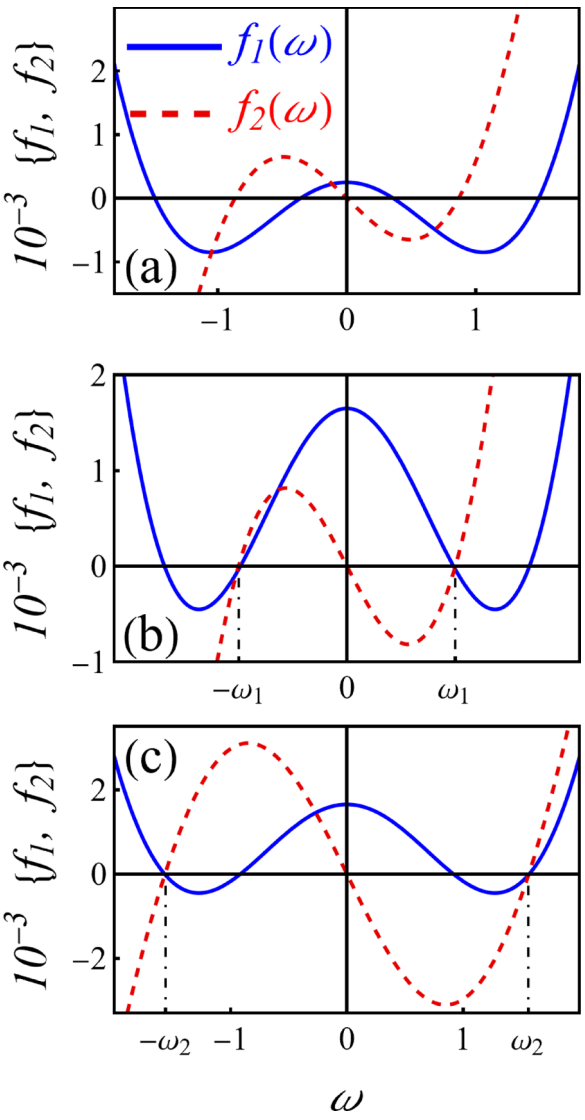

FIG. 4. The run of the curves $f_1(\omega)$ (solid, blue) and $f_2(\omega)$ (dashed, red). (a) The generic case with the different roots of the equations $f_1(\omega) = 0$ and $f_2(\omega) = 0$. (b) The case of the coincidence of the root of $f_2(\omega) = 0$ with the smaller root ω_1 of the equation $f_1(\omega) = 0$. (c) The coincidence of the root of the equation $f_2(\omega) = 0$ with the larger root ω_2 of the equation $f_1(\omega) = 0$. The dot-dashed line indicates the root position.

2. Relations between $f_1(\omega)$ and $f_2(\omega)$ leading to the bifurcation

It is easy to plot $f_1(\omega)$ and $f_2(\omega)$, helping one to understand the behavior of Eqs. (47) qualitatively.

Figure 4(a) displays a generic view of $f_1(\omega)$ and $f_2(\omega)$ behavior as the functions of the dimensionless frequency ω when j, λ, and v are not related to one another. In this case, (46) as well as (47) have no solution.

Two examples of the situation with the solution of the system of Eqs. (47) are shown in Figs. 4(b) and 4(c). One concludes that to give a solution to Eq. (46), the functions $f_1(\omega)$ and $f_2(\omega)$ must exhibit at least one pair of roots $\pm\omega_0 \neq 0$ each.

The root $\omega = 0$ of the system (47) corresponds to the formation of the constant overcritical solution, independent

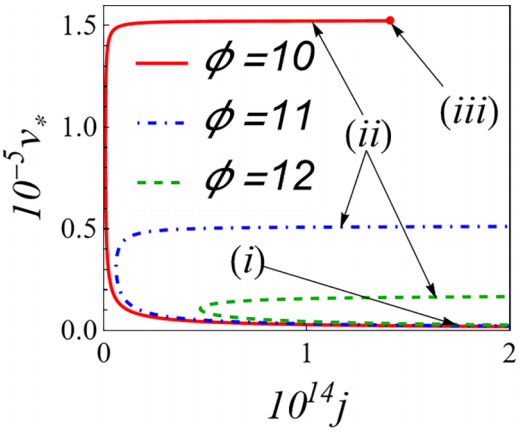

FIG. 5. Dependence of the dimensionless isotherm velocity of the bifurcation v_* on the dimensionless temperature gradient j. The solid line corresponds to $\phi = 10$, the dot-dashed line to $\phi = 11$, and the dashed one to $\phi = 12$. One separates the lower, first bifurcation velocity v_{*1} indicated by (i) and the upper, second one v_{*2} indicated by (ii). The periodic solution takes place only at $v_{*1} \leqslant v \leqslant v_{*2}$. The upper branch of the curve $\phi = 10$ ends up in the point $v = v_{\max}$ indicated by (iii). In the other cases, such points also exist, situated outside of the field shown in the image.

of t. The formation of such a solution does not describe any bifurcation, and we disregard it.

The bifurcation condition requires that two equations, $f_1(\omega_0) = 0$ and $f_2(\omega_0) = 0$, are satisfied at some value of the frequency $\omega_0 \neq 0$. That is, a pair of the roots $\pm\omega_0$ of $f_1(\omega)$ must coincide with those of $f_2(\omega)$.

Figures 4(b) and 4(c) show the particular cases of the coincidence of the roots. The latter imposes a condition on the parameters j, λ, v, and ϕ.

C. The critical velocities

Solving the system (47) one obtains two pairs of solutions:

$$\frac{j_*}{\lambda} = \frac{4(v^2-8)(v^2-6)(v^2+4)A - 5(v^2+4)^{5/2}(3v^2-16)A^2}{16(v^2-6)^2}$$

$$\omega_*^2 = \frac{(v^2+4)^2}{4v(v^2-6)}\left[\frac{(v^2+4)^{3/2}}{2\lambda\sqrt{p(\phi)\ln(v_{\max}/v)}} - 4v\right]. \tag{48}$$

For brevity, we introduced A as follows:

$$A = \frac{1}{2\lambda v\sqrt{p(\phi)\ln(v_{\max}/v)}} - \frac{4}{(v^2+4)^{3/2}}.$$

In principle, the first equation (48) yields the value of the dimensionless temperature gradient j_* corresponding to the bifurcation at a given isotherm velocity v. The second equation (48) gives the frequency of the solution (45) branching off in this point.

In experiments, however, the convenient parameter controlling the bifurcation is the isotherm velocity v, the bifurcation taking place at $v = v_*$. One can consider the first Eq. (48) as the dependence $v_* = v_*(j/\lambda)$ in the parametric form. Figure 5 shows such a dependence for $\phi = 10$, 11 and 12.

One observes that each curve $v_*(j)$ has a form of a hairpin. One distinguishes its lower branch, v_{*1}, and the upper one, v_{*2}. In the following, we refer to them as the first and the second critical velocities. In Fig. 5 the former and the latter are indicated by (i) and (ii) correspondingly. The periodic solution (45) is possible only within the interval $v_{*1} \leqslant v \leqslant v_{*2}$.

Further, the upper branch ends up in the point $v_{*2} = v_{\max}$ (34). This point is visible only in Fig. 5, at the curve $\phi = 10$ indicated by the arrow (iii). The upper branch does not continue beyond this limit point. In the cases $\phi = 11$ and 12, such limit points also exist at the upper branches of the corresponding curves. However, they are situated outside the image and, therefore, are invisible in Fig. 5.

At $v_{*1} < v_{\max}/10$, in the region indicated by the arrow (i) Fig. 5, the first critical velocity exhibits the asymptotic behavior:

$$v_{*1} \approx (m_1 + m_2\phi^{5/2})j^{-0.574}, \tag{49}$$

where $m_1 \approx 2.04$ and $m_2 \approx 3.8 \times 10^{-3}$. We obtained this approximate analytical expression by numerical least square fitting as described in Appendix C in detail. Returning to the original variables (16) and (17) one finds the following expression for the first critical velocity:

$$V_{*1} \approx (m_1 + m_2\phi^{5/2}) \times \frac{\Gamma^{0.787}\Theta_b^{0.574}\chi^{0.213}}{J^{0.574}}. \tag{50}$$

From our solution Fig. 5, one can notice that the relation $v_{*2} \approx v_{\max}$ gives a good approximation for v_{*2}. In the original variables, the second critical velocity takes the following form:

$$V_{*2} \approx \frac{\sqrt{\chi\Gamma}}{n}(\phi + 2 - \sqrt{\phi(\phi+4)})\exp\left[-\frac{2\phi}{\sqrt{\phi(\phi+4)}-\phi}\right] \tag{51}$$

taking place at

$$\Theta_{\max} = \frac{\Theta_b}{2}(\sqrt{\phi(\phi+4)} - \phi). \tag{52}$$

As we described in Sec. IV C at $V > V_{\max}$ the conditions of bifurcation (46) are not valid anymore. Therefore, it is this point that corresponds to the second critical velocity $V_{*2} \approx V_{\max}$ at which the stick-slip motion vanishes.

D. The necessary conditions of the bifurcation

Several inequalities yield the necessary conditions for bifurcation. They are derived in Appendix D. The most important is the following one:

$$v \geqslant 2\sqrt{2}. \tag{53}$$

Its consequences we discuss here.

1. The second critical velocity and the restriction placed on Γ

As we have already discussed in Sec. IV C, the bifurcation takes place in the automodel regime, that is, at $v \leqslant v_{\max}$. The latter requires $v_{\max} > 2\sqrt{2}$. Together with (51) this yields the condition

$$n \leqslant \frac{1}{4\sqrt{2}}(\phi - \sqrt{\phi^2+4\phi} + 2)\exp\left(-\frac{2\phi}{\sqrt{\phi^2+4\phi}-\phi}\right). \tag{54}$$

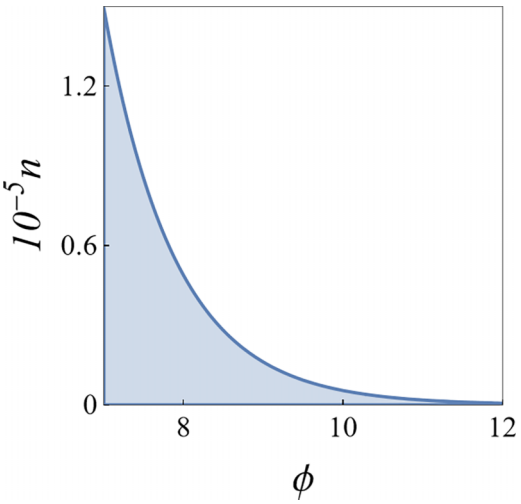

FIG. 6. The bifurcation occurs only within the plane's shaded domain (ϕ, n).

Figure 6 shows the shaded domain in which the inequality (54) holds. According to (17) the condition (54) imposes the limitation on the value of Γ, namely,

$$\Gamma \lesssim 0.35\left(\frac{\alpha_0\Theta_b}{K_0\beta}\right)^2\frac{\gamma G}{\chi}(\phi-\sqrt{\phi^2+4\phi}+2)^2 \times \exp\left(-\frac{4\phi}{\sqrt{\phi^2+4\phi}-\phi}\right).$$

The latter conclusion qualitatively agrees with the experimental observation on $PbTiO_3$ reported in [4] according to which with passing from glass to metallic substrate (that is, from a smaller to a considerably large Γ), the jerky phase front motion vanishes.

The necessary condition for the instability related to hysteresis. One can formulate another significant inequality restricting the phase transformation's thermal parameters, making the bifurcation possible. It is related to the condition of scenario (d): $\Theta_{max} > \Theta_{low}$. One can rewrite it in a more convenient form,

$$(\Theta_b - \Theta_{max})/\Delta\Theta_h > 1. \tag{55}$$

Using (52) one finds

$$\frac{\Theta_b - \Theta_{max}}{\Delta\Theta_h} = \frac{\Theta_b}{2\Delta\Theta_h}[\phi + 2 - \sqrt{\phi(\phi+4)}]. \tag{56}$$

Recalling the ϕ definition (17) and making use of (56) and (55) one separates out the domain in the space $(\Theta_b, \Delta\Theta_h, \epsilon)$ where the stick-slip instability is possible. It is shown in Fig. 7(a). The necessary condition of the bifurcation (55) holds in its shaded domain.

Figure 7(b) shows the cross sections of the surface displayed in Fig. 7(a) by the planes $\Theta_b = 100$, 300, and 700 K. The domain below the corresponding curve admits the bifurcation.

2. The first critical velocity

Let us apply the inequality (53) to the first critical velocity. If $v_{*1} > 2\sqrt{2}$ and the bifurcation is supercritical (soft), the solution (48) holds, and the first critical velocity is accurately described by the approximate expression (50).

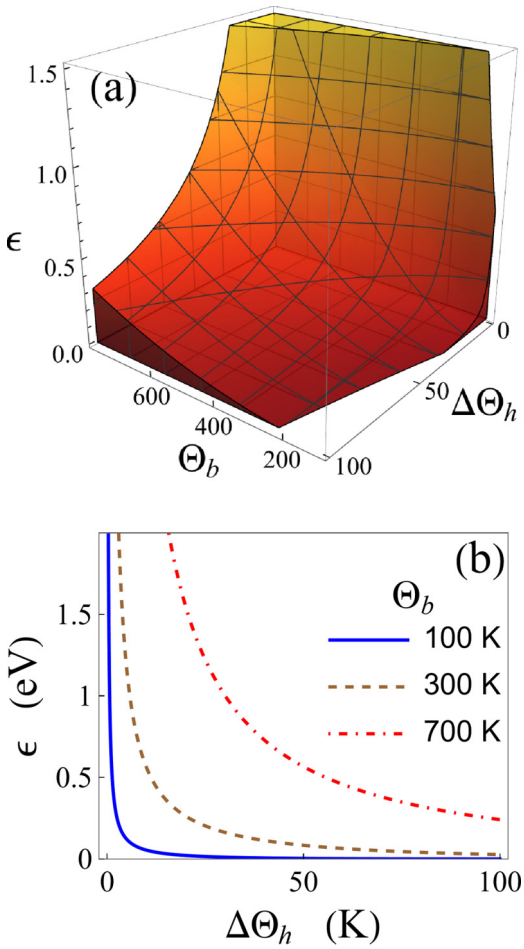

FIG. 7. (a) The domain of the parametric space $(\Theta_b, \Delta\Theta_h, \epsilon)$ where the scenario (d) can take place. Θ_b and $\Delta\Theta_h$ are given in degrees Kelvin, and ϵ is in electronvolts. (b) Cross sections of the 3D domain are shown in (a) by the planes $\Theta_b = 100$ K, 300 K, and 700 K.

If $(m_1 + m_2\phi^{5/2})j^{-0.574} < 2\sqrt{2}$, the bifurcation can take place only at $v = v_{*1} = 2\sqrt{2}$. In this case, the bifurcation becomes subcritical (hard). One describes the first critical velocity during this subcritical bifurcation as follows: $v_{*1} = 2\sqrt{2}$, yielding

$$V_{*1} = 2\sqrt{2\chi\Gamma}. \tag{57}$$

Let us observe that the expression for the first critical velocity is independent of any parameters of Landau potential or, equivalently, anyone characterizing the $\dot{X}(\Theta)$ curve. More precisely, its single relation to this curve is that this instability occurs only if the process belongs to the ascending rather than the descending branch.

Thus V_{*1} in (57) depends only on χ and Γ defining the heat removal rate. The latter points out the instability mechanism at $V = V_{*1}$. Namely, *provided at the ascending branch, instability occurs as soon as the heat has no time to evacuate.*

E. The role of the activation energy

In Appendix D we give rigorous proof that the bifurcation with the formation of the self-oscillating solution is possible only for $\mu > 0$. Since at $\phi = 0$ one finds $\mu = -n < 0$, the inequality $\mu > 0$ can hold only at $\epsilon > 0$. The value $\phi = 0$ corresponding to $\epsilon = 0$ describes the transitions of the displacive type. The latter qualitatively differs from the case $\phi > 0$ ($\epsilon > 0$) characteristic for the order-disorder transformations.

This brings us to the most important conclusion of the present work: *the stick-slip propagation of the phase front is the fingerprint of the order-disorder phase transition*.

VI. COMPARISON OF THE THEORETICAL AND EXPERIMENTAL RESULTS

A. Displacive versus order-disorder transitions

For many years, research has insisted that perovskites (including the lead titanate) exhibit the phase transformation of the displacive type [36,37]. During the last few decades, however, modern experimental techniques have enabled one to unequivocally establish a pronounced order-disorder component in many materials which were previously believed to exhibit the displacive transitions. The order-disorder transition has been revealed, for example, in perovskites, such as $BaTiO_3$ [38–41], $KNbO_3$ [40–42], $PbZrO_3$ [43], and $KCaF_3$ [44]. It has also been discovered in some ferroelectrics-semiconductors, such as GeTe [45], PbTe, PbS [46], and SnTe [47] as well as in borocites [48]. Though the microscopic transition mechanisms in these materials are still a subject of vivid debates, the common opinion is that the order-disorder component plays a vital role in these transformations. For this reason, all these transformations of the order-disorder or hybrid types inevitably involve activation processes.

In particular, the order-disorder nature has been discovered in the classical ferroelectric $PbTiO_3$ [49]. As such, this material must exhibit nonzero activation energy. We discuss it in detail in Sec. VI B below. $NaNbO_3$ also exhibits the order-disorder phase transformation [50] with $\epsilon \approx 0.5$ eV [51]. These findings agree with our conclusion that the self-oscillatory phase front motion can occur only during an order-disorder or hybrid transition.

The above discovery makes one expect more other materials exhibiting such a feature. For such materials, one can use the model developed in the present paper as an alternative approach to proving the existence of a suspected order-disorder component. Indeed, the rise of the oscillational dynamics of the phase front makes sure that the transition inevitably possesses, at least, an order-disorder component. Also, our results offer an accurate method for independent measurement of the activation energy's value. We discuss this approach in the next section.

B. Experiments with $PbTiO_3$ in the light of the present theory

In experiments [2–8] the key material parameter Γ has not been measured, and hinders the possibility of comparing these observations with our results.

As a work around, on the one hand, from the available experimental data, we can estimate the possible value of Γ. On the other hand, for one of the experimentally measurable values, we have found a theoretical expression containing no Γ. The latter enables us to estimate the activation energy of the order-disorder component using available experimental data.

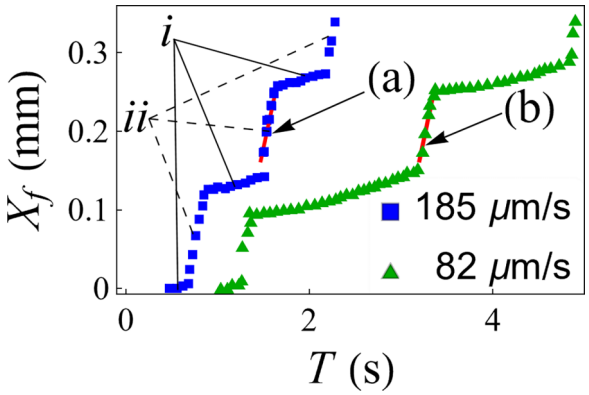

FIG. 8. Examples of the relaxational oscillations of the phase front motion in $PbTiO_3$. Dots are taken from the experiment [6]. The legend gives the isotherm velocity. (i) indicates the slow and (ii) the fast motion phase. The solid lines (a) and (b) fit the high-speed regime of the front motion. Fitting of (a) yields $\dot{X} \approx 544$ μm/s, and (b) gives $\dot{X} \approx 556$ μm/s.

1. *Parameters of* $PbTiO_3$

In Table I we collected parameters of $PbTiO_3$ available from various experiments.

C. The bifurcation in $PbTiO_3$ is subcritical

Using the parameters summarized in Table I and assuming that the bifurcation is soft, we failed to solve Eqs. (48) numerically or graphically. To the best of our knowledge, such a solution with the parameters from Table I does not exist. In the following, we treat the bifurcation as a subcritical one. The latter means that Eqs. (48)–(50) are not applicable. Instead one should use (51) and (57).

1. *On the relation of* V_{*2} *to* $V_{\max}$

On the one hand, a sequence of measurements with increasing isotherm velocities reported in [5] enables one to roughly estimate V_{*1} and V_{*2} in $PbTiO_3$. They revealed that the stick-slip motion first shows up at the isotherm velocity of about 100 μm/s. This value, thus, approximately corresponds to the first critical velocity. With further velocity growth, the jerky motion vanishes as soon as the isotherm velocity reaches about 500 μm/s. The latter value, thus, corresponds to the second critical velocity.

On the other hand, away from the bifurcation point, the self-oscillations necessarily take the relaxational character [34]. Figure 8 displays the experimental points of the phase front position X_f vs time T from the experiment of Dec [6]. It gives two typical examples of the relaxational oscillations of the phase front motion.

The relaxational process consists of a periodic repetition of two phases of motion: starting with the slow one (Fig. 8 i) and followed by a fast one (Fig. 8 ii). The solid lines (a) and (b) shown in Fig. 8 fit the fast relaxational phase by the formula $X_f = X_0 + V_f T$, where the initial position of the front X_0 and

its velocity V_f during the fast phase are the fitting parameters. The fitting shown by Fig. 8(a) yields $V_f \approx 544$ μm/s, while the fitting shown in (b) gives $V_f \approx 556$ μm/s. We also fitted other portions of these curves with the fast relaxation phase to different processes reported in [6] but not shown here, as well as those reported in [7]. In all cases, we obtained the $\dot{X}$ values, close to 500 μm/s, presumably deviating from one another within the experimental error.

Let us stress that we obtained the values of the velocity of the fast relaxational phase close to 500 μm/s for the experiments made with the isotherm speed varying between 43 μm/s, and 313 μm/s as reported in [6]. The latter suggests that the velocity of the fast relaxational phase is independent of the isotherm speed. In contrast, it is determined by the intrinsic properties of the crystal.

During the initial, slow phase of the relaxational oscillation, the front moves slowly over the distance ΔX_s during the time ΔT_s. The following fast phase lasts the time ΔT_f and the front displaces over ΔX_f. The period ΔT is $\Delta T = \Delta T_s + \Delta T_f$. The condition that the front average velocity is equal to the isotherm speed V,

$$V = \frac{\Delta X_s + \Delta X_f}{\Delta T_s + \Delta T_f}, \tag{58}$$

is necessary for the phase front to keep pace with the isotherm. Let us denote $\Delta X_{s,f} = V_{s,f}\Delta T_{s,f}$, where $V_{s,f}$ is the average front velocity during the slow and fast phases correspondingly. One finds the following ratio:

$$\frac{\Delta T_s}{\Delta T_f} = \frac{V_f - V}{V - V_s}. \tag{59}$$

Equation (59) shows that with increasing V the ratio $\Delta T_s/\Delta T_f$ decreases. One sees the example of such behavior in Fig. 8. As soon as $V = V_f$ the ratio $\Delta T_s/\Delta T_f$ turns into zero; that is, at $V_{*2} = V_f$, one finds the bifurcation point where the relaxational stick-slip motion transforms into the steady one.

To obtain the value of V_f and, correspondingly, of V_{*2}, one must solve the system of the nonlinear integro-differential equations (25) and (26). Nevertheless, we can qualitatively reveal its value also without such a solution. During the slow phase, the front stays behind the isotherm, and its lag H_0 gradually becomes considerable. At the beginning of the fast phase, the front accelerates to the velocity V_f somewhat below V_{max} to keep up with the isotherm. As we already discussed, the latter does not exceed V_{max}, since at $V > V_{max}$ the motion takes a nonautomodel form, and its character changes. Analyzing the behavior of the second critical velocity (Fig. 5 ii) and comparing it with the position of the point V_{max} (Fig. 5 ii) one infers that $V_{*2} \approx V_{max}$.

This conclusion enables us to estimate the activation energy of the order-disorder component $PbTiO_3$, which we discuss in the next section.

2. *Activation energy of* $PbTiO_3$

Comparing the maximum front velocity according to the prediction of Gordon's theory [21,22] with his measurements Dec estimated the kinetic factor of $PbTiO_3$ as $K \approx 6.2 \times 10^{-11}$s [7]. Using the relation (8), $K_0 \approx 1. \times 10^{-13}$s, and the Θ_b value taken from Table I, one finds the activation energy $\epsilon \approx 0.42$ eV.

The theory of Gordon, however, does not account for the temperature inhomogeneity, but the latter gives rise to the self-oscillating phase front motion. Thus, this theory can give only a rough estimate of the activation energy. Below we estimate ϵ using the theoretical value V_{*2}.

Let us denote the maximum velocity achieved during the relaxational oscillations of the front velocity in the experiment as $V_{max}^{(exp)}$. Equating V_{*2} (51) to $V_{max}^{(exp)}$ one obtains the following relation:

$$\left[1 + \frac{1}{2}(\phi - \sqrt{\phi(\phi+4)})\right] \exp\left(\frac{2\phi}{\phi - \sqrt{\phi(\phi+4)}}\right) = \frac{n}{\sqrt{\Gamma\chi}} V_{max}^{(exp)}. \tag{60}$$

Using (17) one finds that the ratio $n/\sqrt{\Gamma\chi}$ takes the following form:

$$\frac{n}{\sqrt{\chi\Gamma}} = \frac{0.3K_0\beta}{\alpha_0\Theta_b\sqrt{G\gamma}}.$$

The relation (60) is, thus, independent of Γ, enabling us to estimate ϕ from the experimental data.

From the paper [6] by fitting, one obtains the value $V_{max}^{(exp)} \approx 500$ μm/s (Table I). Making use of the data from Table I one finds $V_{max}^{(exp)} n/\sqrt{\Gamma\chi} \approx 2.94 \times 10^{-7}$. With this value, solving Eq. (60) numerically with respect to ϕ, one finds $\phi \approx 11.51$, yielding

$$\epsilon \approx 0.59\text{eV}.$$

3. *The first critical velocity and* Γ

Self-oscillations starting at zero velocity.. In Sec. V D 2 we have seen that the first critical velocity V_{*1} (57) depends only on the parameters χ and Γ defining the rate of the heat evacuation. In turn, Γ depends on several parameters of the sample, such as its thickness, heat capacity, and conductivity. It is different for different samples, let alone different materials. If the product $\chi\Gamma$ is small, one finds a small V_{*1} value. If it is beyond the experimental resolution, one will observe the self-oscillation regime at all experimentally measurable velocity values within the interval $0 < V < V_{*2}$. It is this case that plausibly takes place in $NaNbO_3$ [5,8,9].

Estimate of Γ *in* $PbTiO_3$. Let us apply the limitation imposed on Γ to $PbTiO_3$. Using the data from the Table I one finds $n \approx 9.01 \times 10^{-7}\sqrt{\Gamma}\text{s}^{1/2}$. Taking the value $\phi \approx 11.51$ obtained in the previous section, one finds the following limitations from the inequality (54):

$$0 \leqslant \Gamma < 0.014\text{s}^{-1}.$$

Since the bifurcation is subcritical, one can use the expression (57) for the first critical velocity. This yields the following Γ value:

$$\Gamma = \frac{V_{*1}^2}{8\chi}. \tag{61}$$

Substituting the V_{*1} and χ summarized in Table I, one finds

$$\Gamma \approx 0.0012\text{s}^{-1}. \tag{62}$$

The latter figure lies within limits established above.

4. The thermodynamical condition of arising of the bifurcation

Substitution of $\phi \approx 11.51$ as well as Θ_b and $\Delta\Theta$ from Table I into the expression (56) yields $(\Theta_b - \Theta_{max})/\Delta\Theta_h \approx 2.29$. Thus, the necessary condition (55) holds.

5. The Biot and Péclet numbers

Using the value (62) obtained above and the definition (10) one finds $\mathrm{Bi} \approx 3 \times 10^{-5}$. Thus, the condition $\mathrm{Bi} \ll 1$ holds.

If the Péclet number is small ($\mathrm{Pe} \leqslant 0.1$), the temperature distribution has enough time to adapt to the temperature variation at the heaters. In this regime, one can regard $\Theta_{furn}(X, T)$ as a linear function, as written in (4). For the $PbTiO_3$ crystal studied in the experiments mentioned above, the condition $\mathrm{Pe} \leqslant 0.1$ (2) and the data from Table I yield the requirement of $V \lesssim 65$ μm/s. However, most of experiments [2–8] employed larger isotherm velocities.

At larger velocities, the distribution $\Theta_{furn}(X, T)$ must differ from the linear dependence. Our numerical simulations (not shown here) suggest that one expects that in this case, the expression $\overline{J} = (\Theta_2 - \Theta_1)/d_1$ is valid for the average gradient $\overline{J}$, rather than for the exact one J. The exact gradient $J = J(X)$ is greater close to the butt ends of the sample but smaller at the isotherm. In addition, it varies during the process. In general, the problem becomes more complex and requires a numeric solution.

VII. DISCUSSION

A. Admissibility of using Gordon's velocity expression

To derive Eq. (23), we used Gordon's expression for velocity of the phase front (20). This expression is exact only in the case of the homogeneously overcooled crystal. We, however, study a crystal subjected to the temperature gradient J. The use of Gordon's velocity is justified, provided the temperature gradient causes a small variation of the order parameter.

One estimates the temperature difference between the phase front and the left sample butt end as follows: $\Delta\Theta \sim Jl \sim Jd_1$. Here l is the distance from the left sample end to the phase front. The typical value of the gradient J used in [3,6] is about a few degrees per millimeter. The typical size d_1 of the crystal is a few millimeters. With such values, one finds the temperature variation $\Delta\Theta \lesssim 1$ K.

Let us estimate the value of the order parameter at the left butt end of the sample. It yields the boundary condition for Eq. (7). One obtains the latter assuming $\partial\eta/\partial T \approx \partial\eta/\partial X = 0$ in (7):

$$\alpha_0(\Theta - \Theta_c)\eta - \beta\eta^3 + \gamma\eta^5 = 0$$

yielding

$$\eta^2(\Theta) = \frac{\beta + \sqrt{\beta^2 - 4\alpha_0\gamma(\Theta - \Theta_c)}}{2\gamma}. \tag{63}$$

At the isotherm, the temperature is equal to that of the binodal Θ_b. Therefore, one can estimate the temperature Θ_{butt} at the butt end as $\Theta_{butt} \approx \Theta_b + \Delta\Theta$. From Table I, one sees that $\Delta\Theta \ll \Theta_b$ and $\Delta\Theta \ll \Theta_b - \Theta_c$. The latter enables one to expand (63) in series in terms of $\Delta\Theta$. Using the binodal position $\zeta = 3/16$ and the explicit expression for ζ (21), one finds $\eta(\Theta_{butt}) \approx \eta_0 + \Delta\eta$, where $\eta_0 = (3\beta)^{1/2}/2\gamma^{1/2}$ and $\Delta\eta = -2\alpha_0\Delta\Theta\gamma^{1/2}/3^{1/2}\beta^{3/2}$. Their ratio is

$$\frac{\Delta\eta}{\eta_0} = \frac{4\alpha_0\gamma}{3\beta^2}\Delta\Theta.$$

Using the data from Table I and the above estimate for $\Delta\Theta$, one finds $\Delta\eta/\eta_0 \lesssim 10^{-1}$. Thus, in the experiments we address, the maximal variation of the order parameter due to the temperature spatial inhomogeneity is relatively small. The latter justifies the application of Gordon's velocity for derivation (23).

B. The instability mechanisms

1. The thermal instability

In this paper, we analyzed the thermal mechanism of forming the stick-slip instability of the front propagation. The possibility of the instability is related to two independent conditions: (1) the $V = V(\Theta)$ dependence must have the ascending and descending branches and (2) the conditions at the beginning of the motion must place the system onto the ascending branch.

The slope $dV/d\Theta$ of the ascending branch is low at a small temperature [as in point ii Fig. 3(d)] but increases with increasing Θ. It decreases again in the vicinity of the point of maximum of the curve $V = V(\Theta)$ [the point v Fig. 3(d)]. The thermal conductivity has enough time to evacuate the liberating heat at a shallow slope. As a result, the front propagates steadily. In Fig. 3(d) the steady propagation takes place between the points indicated by iii and iv. At the latter point, the slope becomes so steep that the heat has no time to dissipate. The latter has the effect of accelerating the front: instability occurs.

If the instability is soft, the front acceleration vanishes as soon as it achieves point vi in Fig. 3(d), where the slope $dV/d\Theta$ becomes small again. Here the liberating heat becomes smaller and, thus, again has time to dissipate.

At $V_{*1} < V < V_{*2}$, the oscillations can gradually take a relaxational character. The latter exhibits slow and fast phases. During the fast phase, the front velocity V_f is close to V_{max}. At $V_{*2} = V_f \approx V_{max}$ the relaxational stick-slip front motion transforms into the steady one.

2. The surface pinning

Under generic conditions, we hypothesized that pinning of the phase front by the surface defects at the left butt end of the crystal represents the necessary condition to observe the regular stick-slip motion. It is the pinning that represents the most probable mechanism for placing the process on the ascending branch of $V(\Theta)$ during the first-order phase transformations.

Indeed, Dec reported that he observed the front starting its motion from the state of rest with the finite velocity [5,6]. The plots $X = X(T)$ reported in [3,9] also testify to such behavior. These observations directly confirm the pinning at the surface or in bulk, close to the left butt end surface. The initial velocities reported in [5,6] were considerably smaller than those observed in [3]. This is due to the difference in the surface defect structure of the crystals studied in these experiments.

3. The stick-slip motion due to pinning in the bulk

Let us briefly discuss the qualitative influence of stationary bulk defects on the front dynamics.

First, let us recall that to set the phase front in motion, one has to apply to it a driving force $F = \varsigma(\Theta_b - \Theta_f)$ related to the overcooling $\Theta_b - \Theta_f$ with the front temperature Θ_f smaller than the binodal temperature Θ_b [cf. Eq. (22)]. Applying an infinitesimally small overcooling to a defectless crystal ($\Theta_b - \Theta_f \to +0$) gives rise to phase front propagation with an infinitesimally low speed ($V_f \to +0$). It gradually increases with overcooling. In crystals containing bulk pinning defects, the front behavior is different.

One finds the following picture in crystals containing uniformly distributed weak pinning defects. These hinder the front motion, their effect resembling a dry friction force. In other words, to break the front free from such defects, one has to apply a driving force F exceeding a critical value F_p. The front, thus, starts propagating only at $\Theta_f < \Theta_b - F_p/\varsigma$ with a finite velocity. One observes that if $F > \varsigma(\Theta_b - \Theta_{max})$ (or equivalently $\Theta_f < \Theta_{max}$), the front is overcooled such that one finds it at the ascending branch of the $V(\Theta)$ curve. Such a situation brings one to the scenario discussed in Sec. VII B 2.

One expects a different scenario in dirty crystals containing strong, loosely distributed pinning defects. If there are no strong surface pinning defects, the front slips off from the crystal butt end unimpeded and starts following the isotherm. One concludes that this mechanism allows the stick-slip motion to start with an infinitely small isotherm velocity. The front propagates until it hits the first pinning center. Such a center with one or a few defects can completely arrest the phase front. The latter dwells on the center until F exceeds F_p. After that, the front leaves the center. No first critical velocity takes place in this scenario. According to (22), the overcooling increases with the isotherm velocity: $F = \varsigma(\Theta_b - \Theta_f) = V$. The front breaks free as soon as the driving force becomes equal to the force of pinning F_p. At this moment, one finds it at a distance ΔX behind the isotherm. To overtake the isotherm, the front develops stronger overcooling such that the speed V_f exceeds V. The distance ΔX in this scenario is equal to the front spatial jump.

Let us note that both positions of the pinning centers and the values of their pinning force F_p are scattered. This implies that the lag ΔX, the time intervals ΔT between the front arrests, and the velocities V_f also take the nonequal values. However, the values ΔX and ΔT may considerably differ, while all V_f values, though different, lie close to the maximal value V_{*2} the front can achieve. The arbitrary values of ΔX and ΔT make the stick-slip process irregular and aperiodic. Further, the amount and distribution of the defects unpredictably vary from sample to sample. One can expect, therefore, the stick-slip front motion of this origin to be observable in some samples and absent in others.

References [5] and [9] reported the observation of strongly scattered ΔX and ΔT values and less scattered V_f values on $NaNbO_3$. These observations agree with the picture of strong bulk pinning defects.

One concludes that both mechanisms act in a concerted fashion. In $PbTiO_3$, the transformation heat is high, while in $NaNbO_3$, it is relatively low. Consequently, the thermal mechanism dominates the instability in the former, while the defect mechanism in the latter.

C. Relationship to the previous results

In the papers of Roitburd and Umantsev [24,25] as well as in those of Gordon [21–23] no temperature gradient has been accounted for. As the immediate cause of the phase front propagation, these works regarded only the homogeneous overcooling or overheating of the whole sample. This distinguishes the papers [21–25] from the studies of Kurtze, van Saarloos, and Weeks [17,18], and the present one where the temperature gradient role is explicitly accounted for.

Umantsev has found that the front propagation's oscillatory regime can never occur in all solids without exceptions. This conclusion relates to the limitation of the model studied in [25]. Umantsev and Roitburd derived the $V(\Theta)$ dependence in the framework of the weakly nonequilibrium thermodynamics, the dependence of kinetic coefficients on temperature assumed to be negligible. The latter excludes any activation process [24,25]. Translating into our language, they analyzed the case of the transformation of the displacive type $\epsilon = 0$. For these materials, our conclusions coincide with those of Umantsev, while the necessary condition of the stick-slip motion is $\epsilon > 0$.

In a series of papers [15–18], Kurtze, van Saarloos and Weeks studied directional crystallization of amorphous semiconductors. They analyzed both the case of no external temperature gradient and its presence. In the latter case, it was generated by the laser spot. The latter scanned the sample with a fixed velocity V. Like in [14], they used a phenomenological algebraic relation of the activation type between the front velocity and temperature.

In these papers, conditions of self-oscillations emergence during the explosive crystallization have been established, and its characteristics were determined [15–18]. In many respects our results resemble their findings.

Indeed, the origin of the instability at low isotherm velocity $V = V_{*1}$ during the explosive crystallization and crystal-crystal phase transformation are the same; namely, the process occurs under the propagating temperature gradient in both cases. The laser spot generates the gradient during explosive crystallization. In the crystal transformation case, one forms it by the furnace. Further, in both cases, the instability source is the positive feedback: the bifurcation requires the existence of the ascending branch of $V(\Theta)$. The process must belong to this branch. In particular, we obtained the expression for the first critical velocity V_{*1} (57) identical to that obtained in [16]. It is the expected coincidence since this instability is independent of the transition nature (see the discussion in Sec. V D 2).

However, the nature of the crystal-crystal transformations dramatically differs from the transition from the amorphous to crystal phase.

Indeed, first, the amorphous-to-crystal transition exhibits no hysteresis. Second, only the ascending $V(\Theta)$ branch exists for the amorphous-to-crystal transition [see Fig. 1(a) in [17]]. Third, in [15–18] (as well as in [14]) the curve $V(\Theta)$

expression has been hypothesized from the phenomenological considerations, rather than derived.

Contrary to that, we derived the specific relation $V = V(\Theta)$ (23) valid for the first-order crystal-crystal phase transformations. It establishes $V(\Theta)$ in terms of the coefficients of Landau potential already determined for many materials [52]. This enabled us to apply our theory to discuss experiments [2–8] on $PbTiO_3$. Our results also apply to many other crystals with experimentally known Landau coefficients.

Further, during the structural phase transitions, the process takes only place within the hysteresis region. The interplay of the hysteresis width and the specific $V(\Theta)$ form gives rise to four different scenarios of the phase transformation kinetics, rather than the single fast mode of the explosive crystallization behavior.

Next, for the transitions of the order-disorder type, one finds both the ascending and the descending $V(\Theta)$ branches [see Figs. 3(b)–3(d)], separated by the maximum point. The latter is closely related to the instability at the second critical velocity V_{*2}.

Let us briefly mention a few essential differences in the physical nature between explosive crystallization and crystal-crystal transformation.

First, in glass, only the ascending branch is available. Hence, the process automatically finds itself at the ascending branch, prone to instability at V_{*1}. In contrast, the gradient furnace always brings the process to the descending part of $V(\Theta)$. This excludes positive feedback and instability.

The process can occur only at the ascending branch, provided something forces the phase front to stay motionless at the sample boundary until the driving force becomes considerable. In this case, it further moves along the ascending $V(\Theta)$ branch and exhibits the instabilities.

This brings us to the hypothesis of the crucial role of surface pinning defects. We argue that without such defects one cannot explain the experimental observations [2–9]. Second, in these two classes of transformations, the increase of the temperature at the front differ by about two orders of magnitude. This difference gives rise to a significant discrepancy in the values of the phase front velocities. In particular, in the case of explosive crystallization, the front velocities reach several meters per second. At the same time, during the structural phase transitions, they are several orders of magnitude lower (see Table I).

Propagation of a reaction front during gasless fuel combustion also represents a process comparable to those studied in this paper as well as in [15–18]. During such combustion, one has experimentally discovered a transition from the steady to self-oscillatory flame propagation regime [12]. The theoretical value for the instability threshold $V_{\rm th}$ of the combustion front propagation has been obtained in [19]. "Translating" notations of [19] into our "language," one makes sure that the instability thresholds are literarily identical: $V_{\rm th} = V_{*1}$ (57), and also equal to one found by Saarloos and Weeks [16]. We discussed the origin of their coincidence in Sec. V D 2.

A more detailed comparison of the kinetics of the first-order phase transformations, amorphous crystallization, and gasless combustion is an extensive task out of the scope of this paper.

VIII. SUMMARY

To summarize, we report a theoretical study of a non-isothermal propagation of a phase front driven by a moving temperature gradient. We prove that for the phase transformations of the displacive type, the phase front always steadily follows the isotherm.

In the case of the order-disorder or hybrid phase transformations, we argue that the stick-slip instability can show up only provided surface defects have initially pinned down the phase front at the beginning of its motion. We find the first critical velocity of the isotherm at which the steady front motion becomes unstable and the stick-slip motion arises. We further determine the second critical velocity. The jerky motion vanishes as soon as the isotherm velocity exceeds the latter. We state that the self-oscillatory propagation is a fingerprint of the order-disorder or hybrid transformations. Our calculations enabled us to extract the activation energy of the order-disorder degree of freedom responsible for the phase transformation from the measurements of the driven motion of the phase front. We further discuss the measurements performed on $PbTiO_3$ and $NaNbO_3$ in light of our results.

APPENDIX A: EVOLVING HEAT AND THE RESCALED THERMAL EQUATION

Rescaling (16) transforms the thermal equation (12) as follows:

$$\frac{\partial \delta\Theta}{\partial t} = \frac{\partial^2 \delta\Theta}{\partial x^2} - \delta\Theta + \frac{\Lambda}{c\Gamma}. \tag{A1}$$

Following [24], one writes the evolving heat as the sum of two terms::

$$\Lambda = \Lambda_1 + \Lambda_2 = \alpha_0 \Theta \eta \frac{\partial \eta}{\partial T} + K\left(\frac{\partial \eta}{\partial T}\right)^2. \tag{A2}$$

The first term (A2) describes the transformation heat, and the second one the heat generated due to the order parameter evolution [24]. Assuming that the phase front propagates with the velocity V one finds $\partial\eta/\partial T \sim V\partial\eta/\partial X \sim V\eta/\delta$, where δ is the phase front width. One estimates $\Lambda_1 = \alpha_0\Theta\eta\partial\eta/\partial T \sim \alpha_0\Theta_{\rm b}V\eta^2/\delta$ and $\Lambda_2 = K(\partial\eta/\partial T)^2 \sim KV^2\eta^2/\delta^2$. Using the parameters from Table I and $\delta \sim 120$ Å [7], one finds that at $K \lesssim 3\times 10^{-3}$s, the following inequality holds:

$$\frac{\Lambda_1}{\Lambda_2} \sim \frac{\alpha_0\Theta_{\rm b}\delta}{KV} \gg 1. \tag{A3}$$

Therefore, in the following, we omit the second term in (A2). One finds

$$\Lambda \approx -\alpha_0\Theta\dot{X}(T)\eta\frac{\partial\eta}{\partial X}. \tag{A4}$$

Further, the width of the temperature distribution, $(\chi/\Gamma)^{1/2}$, may have any value. However, typically one finds

$$\delta \ll (\chi/\Gamma)^{1/2}. \tag{A5}$$

In this limit, one can accurately approximate the order parameter spatial distribution with the Heaviside function $\theta_{\rm H}(X)$. That is, $\eta(X,T) \approx \eta_0\{1-\theta_{\rm H}[X - X_{\rm f}(T)]\}$, where η_0 is the solution (63) of the homogeneous Landau equation at

the binodal, $\Theta = \Theta_b$:

$$\eta_0 = \left(\frac{\beta}{2\gamma}\right)^{1/2}. \tag{A6}$$

In this case, $\eta\partial\eta/\partial X \approx -\eta_0^2\delta(X - X_f(T))/2 = -\eta_0^2(\Gamma/\chi)^{1/2}\delta[x - x_f(t)]/2$, where the δ function, $\delta(x)$ should not be confused with the phase front width δ.

APPENDIX B: ELIMINATION OF $\delta\Theta$

Representing the solution $\delta\Theta(x,t)$ of the equation (19) in terms of the Green function $\mathfrak{G}(x,t)$ one finds

$$\delta\Theta(x,t) = \Lambda\int_{-\infty}^{t}\mathfrak{G}[x - x_f(t''), t - t'']\dot{x}_f(t'')\,dt''. \tag{B1}$$

We replace the variable t'' by $t' = t - t''$, and calculate the temperature perturbation (B1) $\delta\Theta(x_f(t),t)$ at the phase front $x = x_f(t)$. One finds

$$\delta\Theta(x_f(t),t) = \Lambda\int_0^{\infty}\mathfrak{G}[x_f(t) - x_f(t - t'), (t - t')] \times \dot{x}_f(t - t')\,dt'. \tag{B2}$$

It is convenient to represent the Green function $\mathfrak{G}(x,t)$ in the following form:

$$\mathfrak{G}(x,t) = \int_{-\infty}^{\infty}\exp[-(q^2+1)t + iqx]\frac{dq}{2\pi}. \tag{B3}$$

That is, we applied the Fourier transform for the coordinate x, but not the time t. Substituting (B3) into (B2) one obtains Eq. (26).

APPENDIX C: A SEMIANALYTICAL SOLUTION FOR THE FIRST CRITICAL VELOCITY

We look for the semianalytical solution for the lower branch of the critical velocity at $v_{*1} < v_{max}/10$. The solution $v_{*1} = v_{*1}(j)$ can be obtained parametrically from the expression (48). Dots in Fig. 9(a) show the example of such a solution in the case of $\phi = 12$.

One can accurately approximate the lower branch of this solution by the simple formula $v_{*1} \approx mj^{-0.574}$, where m is the fitting parameter. Figure 8(a) shows by the solid line the fit of the part of this solution, where $v_{*1} < v_{max}/10$. In this case, it yields $m \approx 0.366$.

We made such a fitting for $\phi = 5, 6, \ldots, 12$, and obtained $m = m(\phi)$ in each case. Figure 9(b) displays the obtained values $m(\phi)$ (dots) and their fitting by the expression $m = m_1 + m_2\phi^{5/2}$. This brings one to the expression (49).

APPENDIX D: PROOF OF SOME INEQUALITIES

1. The limitation imposed on the velocity

At small velocity values, the function $f_1(\omega, v)$ has a single minimum at $\omega = 0$. As soon as v exceeds a critical value v_{cr} two sidewise minimums split away from the point $\omega = 0$, while this point becomes maximum (Fig. 8). The critical value $v = v_{cr}$ one determines from the condition $\partial f_1(\omega)/\partial\omega = 0$ together with $\partial^2 f_1(\omega)/\partial\omega^2 = 0$ taken at $\omega = 0$. The former

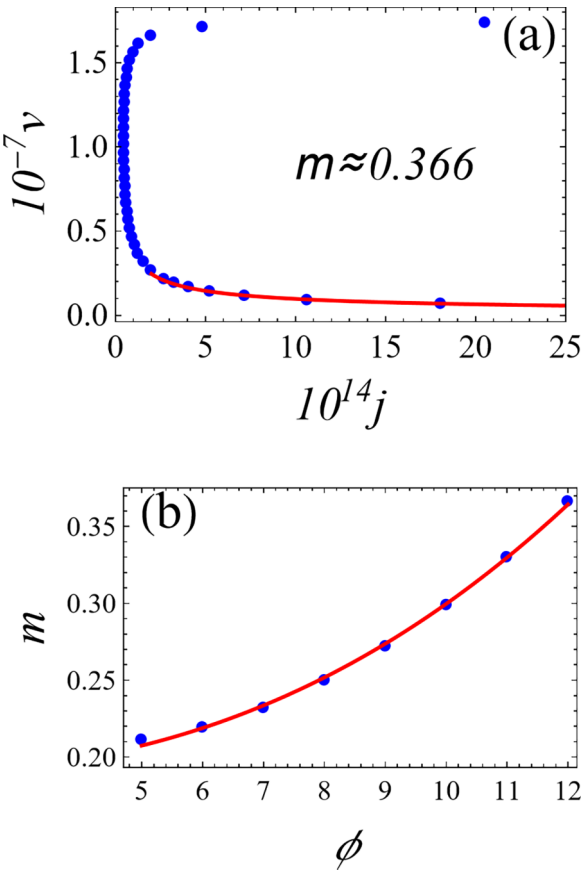

FIG. 9. (a) The solution $v_*(j)$ and its approximation by the expression (49). Dots show the parametric solution $v_* = v_*(j)$. This example corresponds to $\phi = 12$. The solid line displays the fit of the part of this curve $v_* < v_{max}/10$ by the function $v_{*1} \approx mj^{-0.574}$ yielding $m \approx 0.366$. (b) Dots show the values of m obtained by the procedure described in (a) for $m = 5, 6, \ldots, 12$. The solid line fits these points by the formula $m \approx m_1 + m_2\phi^{5/2}$.

expression is automatically fulfilled due to the evenness of $f_1(\omega)$. The latter one yields

$$\left.\frac{\partial^2 f_1(\omega)}{\partial\omega^2}\right|_{\omega=0} = \frac{4(v^2-8)}{(v^2+4)^{5/2}} = 0,$$

whence it follows $v_{cr} = 2\sqrt{2}$. Thus, the bifurcation is possible only at $v > v_{cr}$.

2. The limit imposed on j

According to its definition, $j > 0$. Variation of the parameter j gives rise to the following behavior of $f_1(\omega)$. We show the run of the function $f_1(\omega)$ at small j values in Fig. 10(b) by the solid red line. In this case, $f_1(\omega)$ exhibits two pairs of roots $\pm\omega_1$ and $\pm\omega_2$. As soon as j achieves a value j_{cr} two pairs of the roots fuse [a black, dot-dashed line in Fig. 10(b)], and at $j > j_{cr}$ one finds no roots of $f_1(\omega)$. In this latter case, the system of equations (47) has no solutions. In other words, the bifurcation can happen only at $j \leqslant j_{cr}$. Let us stress that the condition $j \leqslant j_{cr}$ is necessary but not enough. It indicates only the part of the parametric space where the bifurcation

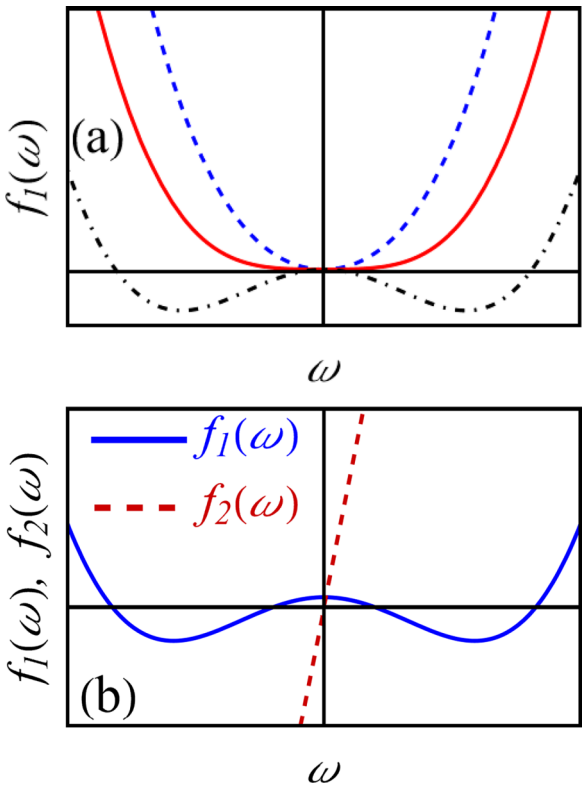

FIG. 10. (a) At small velocity $f_1(\omega)$ exhibits a single minimum at $\omega = 0$ (blue dashed line). At $v = v_{cr}$ this minimum degenerates (solid red line), and at $v > v_{cr}$ two minimums $\omega \neq 0$ split off (black dot-dashed line). (b) Schematic view of the curves $f_1(\omega)$ and $f_2(\omega)$ at $\mu = 0$ (not in scale). (c) Variation of the dependence $f_1(\omega)$ with the increasing j value. At small j, one finds four roots of $f_1(\omega)$. At $j = j_{cr}$ the two pairs of the roots fuse, and at $j > j_{cr}$ $f_1(\omega)$ exhibits no roots.

is not possible, while the first equation (48) represents the sufficient condition of the bifurcation.

One gets the value j_{cr} by solving the following system:

$$f_1(\omega, j_{cr}) = 0$$
$$f_2(\omega, j_{cr}) = 0$$
$$\partial f_1(\omega, j_{cr})/\partial\omega = 0$$

yielding

$$j_{cr} = \frac{\lambda(v^2-8)^2}{10\sqrt{v^2+4}(3v^2-16)}. \tag{D1}$$

One concludes that the bifurcation only takes place at $0 < j \leqslant j_{cr}$.

3. The inequality $\mu > 0$

The requirement $\mu > 0$ for the arising of the bifurcation follows from the properties of the function $f_2(\omega)$. Let us note that above we analyzed the approximate equations (47) valid only at $|\omega| < 2$. For the present proof, we take the exact expression $f_2(\omega) = \mathrm{Im}[\Sigma(\omega, j, \lambda, v)]$ (46). It has the following form:

$$f_2(\omega) = -\frac{\mu\omega}{\lambda v} + f_2^{(1)}(\omega), \tag{D2}$$

where for the convenience, we denoted $f_2^{(1)}(\omega)$ as follows:

$$f_2^{(1)}(\omega) = \frac{2\omega\cos\left[\frac{1}{2}\arctan\left(\frac{4\omega}{v^2+4}\right)\right] - v^2\sin\left[\frac{1}{2}\arctan\left(\frac{4\omega}{v^2+4}\right)\right]}{[(v^2+4)^2+16\omega^2]^{1/4}}. \tag{D3}$$

Let us check the inequality $f_2^{(1)}(\omega) > 0$. One reduces it to the following expression:

$$4\omega > v^2\tan\left[\frac{1}{2}\arctan\left(\frac{4\omega}{v^2+4}\right)\right]. \tag{D4}$$

Further, using the following identity:

$$\tan\left[\frac{1}{2}\arctan(x)\right] \equiv \frac{\sqrt{1+x^2}-1}{x}$$

one comes via (D4) to the simple inequality:

$$2v^2 + y^2 > v^4, \tag{D5}$$

where $y = 16\omega^2/(v^2+4)^2$. From (D5) it follows that $y > v\sqrt{v^2-2}$. Since $v > 2\sqrt{2}$, one concludes that $f_2^{(1)}(\omega) > 0$, that is, it is strictly positive everywhere.

Therefore, at $\omega > 0$ and $v > 0$, the function $f_2(\omega)$ (D2) can turn into zero only due to the first term, provided it is negative. Since $\mu \approx \phi\ln^{-2}(nv)$, and $\phi > 0$, the first term can be negative only if $\mu > 0$. At $\mu = 0$, the function $f_2(\omega)$ has no roots $\omega \neq 0$, and the bifurcation is impossible.

Let us also note that at great values of ω, one finds the following asymptotics:

$$f_2(\omega) \sim -\frac{\mu\omega}{\lambda v} + O(\sqrt{\omega}).$$

Since $\mu > 0$, it exhibits the following asymptotic properties:

$$f_2(\omega) \to \mp\infty \quad \text{at } \omega \to \pm\infty.$$

The behavior of the functions $f_{1,2}(\omega)$ at $\mu = 0$ is shown in Fig. 10(c).

[1] J. C. Burfoot and T. J. Parker, Br. J. Appl. Phys. **17**, 213 (1966).
[2] E. G. Fesenko, M. A. Martynenko, V. G. Gavrilyachenko, and A. F. Semenchev, Izv. Akad. Nauk SSSR, Ser. Fiz. **39**, 762 (1975).
[3] S. M. Yufatova, Y. G. Sindeyev, V. G. Gavrilyachenko, and E. G. Fesenko, Ferroelectrics **26**, 809 (1980).
[4] E. G. Fesenko, V. G. Gavrilyachenko, and A. F. Semenchev, in *Domain Structure of Multiaxial Ferroelectric Crystals* (Rostov University, Rostov-on-Don, 1990) [in Russian].
[5] J. Dec, Ferroelectrics **69**, 187 (1986).
[6] J. Dec, J. Phys. C **21**, 1257 (1988).
[7] J. Dec, Ferroelectrics **89**, 193 (1989).
[8] J. Dec, Phase Trans. **45**, 35 (1993).

[9] J. Dec and V. E. Yurkevich, Ferroelectrics **110**, 77 (1990).

[10] C. E. Wickersham, G. Bajor, and J. E. Greene, Solid State Commun. **27**, 17 (1978); J. C. C. Fan, H. J. Zeiger, R. P. Gale, and R. L. Chapman, Appl. Phys. Lett. **36**, 158 (1980); H. J. Zeiger, John C. C. Fan, B. J. Palm, R. I. Chapman, and R. P. Gale, Phys. Rev. B **25**, 4002 (1982); V. G. Myagkov, JETP Lett. **72**, 4 (2000); I. Smagin and A. Nepomnyashchy, Physica D **238**, 706 (2009); K. Ohdaira, T. Fujiwara, Y. Endo, S. Nishizaki, and H. Matsumura, J. Appl. Phys. **106**, 044907 (2009); K. Ohdaira, N. Tomura, S. Ishii, and H. Matsumura, Electrochem. Solid-State Lett. **14**, H372 (2011); K. Ohdaira, S. Ishii, N. Tomura, and H. Matsumura, J. Nanosci. Nanotechnol. **12**, 591 (2012); K. Ohdaira and H. Matsumura, Thin Solid Films **524**, 161 (2012).

[11] G. C. Egan, T. W. Li, J. D. Roehling, J. T. McKeown, and G. H. Campbell, Acta Mater. **143**, 13 (2018); G. C. Egan, T. W. Heo, A. Samanta, and G. H. Campbell, *ibid.* **179**, 190 (2019).

[12] A. G. Merzhanov, A. K. Filonenko, and I. P. Borovinskaya, Sov. Phys.- Dokl. **208**, 122 (1973).

[13] Yu. M. Maksimov, A. T. Pak, G. B. Lavrenchuk, Yu. S. Naiborodenko and A. G. Merzhanov, Combust. Expl. Shock Waves **15**, 415 (1979); Yu. M. Maksimov, A. G. Merzhanov, A. T. Pak, and M. N. Kuchkin, *ibid.* **17**, 393 (1981); A. V. Dvoryankin, A. G. Strunina, A. G. Merzhanov, *ibid.* **18**, 134 (1982); A. G. Merzhanov and B. I. Khaikin, Prog. Energy Combust. Sci. **14**, 1 (1988); A. G. Merzhanov, in *Combustion and Plasma Synthesis of High-Temperature Materials*, edited by Z. A. Munir and J. B. Holt (VCH, New York, 1990), pp. 1–53.

[14] V. A. Shklovskii, Sov. Phys.-Dokl. **26**, 1155 (1981); Sov. Phys.-JETP **55**, 311 (1982).

[15] W. van Saarloos and J. D. Weeks, Phys. Rev. Lett. **51**, 1046 (1983).

[16] W. van Saarloos and J. D. Weeks, Physica D **12**, 279 (1984).

[17] D. A. Kurtze, W. van Saarloos, and J. D. Weeks, Phys. Rev. B **30**, 1398 (1984).

[18] D. A. Kurtze, Physica D **20**, 303 (1986).

[19] G. M. Makhviladze and B. V. Novozhilov, J. Appl. Mech. Tech. Phys. **12**, 676 (1971).

[20] A Bayliss and B. J. Matkowsky, J. Comput. Phys. **71**, 147 (1987).

[21] A. Gordon, Phys. Lett. A **99**, 329 (1983); Physica B+C **138**, 239 (1986).

[22] A. Gordon, I. D. Vagner, and P. Wyder, Phys. Rev. B **41**, 658 (1990).

[23] A. Gordon, Phys. Lett. A **154**, 79 (1991); Phys. Rev. B **54**, 3055 (1996); A. Gordon and S. Dorfman, *ibid.* **51**, 9306 (1995); A. Gordon, S. Dorfman, and D. Fuks, J. Physique IV (Colloque) **7**, 53 (1997); Philos. Mag. B **82**, 63 (2002); A. Gordon, B. E. Vugmeister, S. Dorfman, and H. Rabitz, Phys. B: Condens. Matter **292**, 257 (2000).

[24] A. R. Umantsev and A. L. Roitburd, Sov. Phys. Solid State **30**, 651 (1988).

[25] A. Umantsev, Physica D **235**, 1 (2007); Modell. Simul. Mater. Sci. Eng. **20**, 045013 (2012).

[26] L. D. Landau and E. M. Lifshitz, *Statistical Physics*, 3rd ed. (Pergamon Press, Oxford, 1985); J. C. Toledano, and P. Toledano, *The Landau Theory of Phase Transitions* (World Scientific, Singapore, 1987); Yu. M. Gufan, *Structural Phase Transitions* (Nauka, Moscow, 1983) [in Russian].

[27] E. Y. Tonkov, *High Pressure Phase Transformations: A Handbook*: Vols. 1–3 (Gordon and Breach, Amsterdam, 1992).

[28] A. V. Lykov, *The Theory of the Thermal Conductivity* (Vysshaja shkola, Moscow, 1967) [in Russian].

[29] T. E. Hooper and A. J. Bell, J. Appl. Phys. **127**, 104102 (2020).

[30] V. G. Bhide, M. S. Hegde, and K. G. Deshmukh, J. Am. Ceram. Soc. **51**, 565 (1968).

[31] G. Shirane and E. Sawaguchi, Phys. Rev. **81**, 458 (1951).

[32] B. M. Foley *et al.*, J. Appl. Phys. **121**, 205104 (2017); E. Langenberg *et al.*, Nano Lett. **19**, 7901 (2019).

[33] D. Kobertz, M. Müller, and A. Molak, Calphad **46**, 62 (2014).

[34] A. A. Andronov, A. A. Vitt, and S. E. Khaikin, *Theory of Oscillators* (Dover Publications, New York, 1987).

[35] M. M. Vainberg and V. A. Trenogin, *Theory of Branching of Solutions of Non-linear Equations* (Noordhoff, Leyden, 1974).

[36] M. E. Lines and A. M. Glass, *Principles and Application of Ferroelectrics and Related Materials* (Clarendon Press, Oxford, 1977); V. G. Vaks, *Introduction into the Microscopic Theory of Ferroelectrics* (Nauka, Moscow, 1973) [in Russian].

[37] Y. Onodera, J. Phys. Soc. Jpn. **73**, 1216 (2004); J. Hlinka *et al.*, Phys. Rev. Lett. **101**, 167402 (2008); I. Ponomareva, L. Bellaiche, T. Ostapchuk, J. Hlinka, and J. Petzelt, Phys. Rev. B **77**, 012102 (2008); E. A. Mikhaleva *et al.*, Phys. Solid State **54**, 1832 (2012); J. Weerasinghe and L. Bellaiche, T. Ostapchuk, P. Kužel, and C. Kadlec, S. Lisenkov and I. Ponomareva, J. Hlinka, MRS Commun. **3**, 41 (2013); M. Paściak, T. R. Welberry, J. Kulda, S. Leoni, and J. Hlinka, Phys. Rev. Lett. **120**, 167601 (2018); I. Tomeno, J. A. Fernandez-Baca, S. Chi, K. Oka, and Y. Tsunoda, J. Phys. Soc. Jpn. **89**, 054601 (2020).

[38] R. Comes, M. Lambert, and A. Guinner, Solid State Commun. **6**, 715 (1968); R. Pirc and R. Blinc, Phys. Rev. B **70**, 134107 (2004); K. Namikawa *et al.*, Phys. Rev. Lett. **103**, 197401 (2009); M. S. Senn, D. A. Keen, T. C. A. Lucas, J. A. Hriljac, and A. L. Goodwin, *ibid.* **116**, 207602 (2016); Y.-T. Shao and J.-M. Zoo, Acta Cryst. B **73**, 708 (2017); S. H. Oh, J. H. Ko, H. Y. Lee, I. Lazar, and K. Roleder, Molecules **23**, 3171 (2018); M. Fontana, N. Kokanyan, and T. H. Kauffmann, J. Phys.: Condens. Matter **32**, 285403 (2020).

[39] A. Bencan *et al.*, Nat. Commun. **12**, 3509 (2021).

[40] S. Ravy, J. P. Itie, A. Polian, and M. Hanfland, Phys. Rev. Lett. **99**, 117601 (2007).

[41] Z. Tan, Y. Peng, J. An, Q. Zhang, and J. Zhu, Inorg. Chem. **60**, 7961 (2021).

[42] V. A. Shuvaeva, K. Yanagi, K. Yagi, K. Sakaue, and H. Terauchi, Solid State Commun. **106**, 335 (1998); K. Tsuda and M. Tanaka, Jpn. J. Appl. Phys. **56**, 10PB09 (2017).

[43] G. Kugel, I. Jankowska-Sumara, K. Roleder, and J. Dec, J. Korean Phys. Soc. **32**, S581 (1998); H. Fujishita and S. Katano, *ibid.* **32**, S202 (1998).

[44] Ph. Daniel, M. Rousseau, and J. Toulouse, Phys. Stat. Sol. (b) **203**, 327 (1997).

[45] P. Fons *et al.*, Phys. Rev. B **82**, 155209 (2010); U. D. Wdowik, K. Parlinski, S. Rols, and T. Chatterji, *ibid.* **89**, 224306 (2014); T. Matsunaga, P. Fons, A. V. Kolobov, J. Tominaga, and N. Yamada, Appl. Phys. Lett. **99**, 231907 (2011); T. Chatterji, S. Rols, and U. D. Wdowik, Front. Phys. **14**, 23601 (2019); C. Wang *et al.*, npj Comput. Mater. **7**, 118 (2021).

[46] E. S. Božin *et al.*, Science **330**, 1660 (2010); K. M. Ø. Jensen, E. S. Bozin, C. D. Malliakas, M. B. Stone, and M. D. Lumsden, Phys. Rev. B **86**, 085313 (2012); B. Sangiorgio, E. S. Bozin, C. D. Malliakas, M. Fechner, A. Simonov, M. G. Kanatzidis,

S. J. L. Billinge, N. A. Spaldin, and T. Weber, Phys. Rev. Mater. **2**, 085402 (2018).

[47] K. R. Knox, E. S. Bozin, C. D. Malliakas, M. G. Kanatzidis, and S. J. L. Billinge, Phys. Rev. B **89**, 014102 (2014); A. Vasdev *et al.*, Sci. Rep. **11**, 17190 (2021).

[48] S. Sueno, J. R. Clark, J. J. Papike, and J. A. Konnert, Am. Mineral. **58**, 691 (1973); P. Felix, M. Lambert, R. Comes, and H. Schmid, Ferroelectrics **7**, 131 (1974); A. T. Shuvaev, I. V. Pirog, and I. A. Zarubin, Physica B **208-209**, 627 (1995); T. I. Nedoseykina, V. A. Shuvaeva, I. V. Pirog, A. T. Shuvaev, K. Yagi, Y. Azuma, and H. Terauchi, Ferroelectrics **284**, 175 (2003); M. N. Iliev, V. G. Hadjiev, M. E. Mendoza, and J. Pascual, Phys. Rev. B **76**, 214112 (2007); V. A. Shuvaeva, K. A. Lysenko, and M. Yu. Antipin, Phys. Solid State **53**, 730 (2011).

[49] R. J. Nelmes, R. O. Piltz, W. F. Kuhs, Z. Tun, and R. Restori, Ferroelectrics **108**, 165 (1990); N. Sicron, B. Ravel, Y. Yacoby, E. A. Stem, F. Dogan, and J. J. Rehr, Phys. Rev. B **50**, 13168 (1994); B. Ravel *et al.*, Ferroelectrics **164**, 265 (1995); J. Kwapulinski, J. Kusz, H. Bohm, and J. Dec, J. Phys.: Condens. Matter **17**, 1825 (2005); R. V. Vedrinskiĭ *et al.*, Phys. Solid State **51**, 1394 (2009); Y. Yoneda and S. Kohara, Ferroelectrics **485**, 34 (2015).

[50] E. Bouziane, M. D. Fontana, and M. Ayadi, J. Phys.: Condens. Matter **15**, 1387 (2003); Yu. I. Yuzyuk *et al.*, *ibid.* **17**, 4977 (2005); L. Jiang, D. C. Mitchell, W. Dmowski, and T. Egami, Phys. Rev. B **88**, 014105 (2013).

[51] K. Konieczny and C. Kajtoch, Ferroelectrics **215**, 65 (1998).

[52] L. Q. Chen, in *Physics of Ferroelectrics: A Modern Perspective, Topics of Applied Physics*, edited by K. M. Rabe, C. H. Ahn, and J. M. Triscone, Vol. 105 (Springer, Berlin, Heidelberg, 2007), p. 363.